Optical absorption spectra of the Holstein molecular crystal for weak and intermediate electronic coupling

M. Hoffmann* and Z. G. Soos
Department of Chemistry, Princeton University, Princeton, New Jersey 08544
(Received 8 March 2002; published 24 July 2002)

We investigate the optical absorption spectrum in a Holstein model for a molecular chain with Frenkel excitons and linear coupling to one internal vibration. The model is extended for nearest-neighbor charge-transfer excitons that mix with the Frenkel excitons. We represent the Hamiltonian in a displaced oscillator (Lang-Firsov) basis and employ a problem-adapted scheme for the truncation of the phonon basis. For weak and intermediate electronic coupling, the complete absorption spectrum and the structure of the relevant eigenstates become accessible by direct numerical diagonalization. We discuss the structure of the phonon clouds and the applicability of the molecular vibron model, in which only joint exciton-phonon configurations are included. As examples, we model absorption spectra of PTCDA (3,4,9,10-perylenetetracarboxylic dianhydride) and MePTCDI (*N*-*N*′-dimethylperylene-3,4,9,10-dicarboximide).

DOI: 10.1103/PhysRevB.66.024305 PACS number(s): 71.35.Aa, 71.38.Ht, 78.40.Me

I. INTRODUCTION

There is revived interest in organic semiconductors based on π-conjugated molecules. The reasons are commercially attractive results in organic LED's (e.g., Refs. 1–5), promising demonstrations of solar cells (e.g., Refs. 6–10) and the fundamental physics of high quality single crystals showing band transport,[11] ballistic hole transport,[12] fractional quantum Hall effects,[13] charge injection lasers,[14] superconductivity,[15] or superconducting switches.[16] Therefore, a detailed understanding of various electronic excitations becomes desirable.

In this article, we investigate the optical absorption spectrum in a Holstein model[17,18] for a molecular chain with Frenkel excitons and linear coupling to one internal vibration. We extend the model to include nearest-neighbor charge-transfer (CT) excitons that mix with the Frenkel excitons. Such a model is approximately realized by some quasi-one-dimensional molecular crystals, in particular by PTCDA (3,4,9,10-perylenetetracarboxylic dianhydride), MePTCDI (*N*-*N*′-dimethylperylene-3,4,9,10-dicarboximide), or related perylene derivatives. PTCDA has become a paradigm because it readily forms highly ordered films,[19,20] while perylene derivatives have solar cells applications.[6,7,9] Several works have sought to understand the PTCDA absorption spectrum and related properties of its electronic excitations.[21–27]

A major advantage of PTCDA-related systems is simple and accessible molecular behavior. The lowest π-π^* excitation is dipole allowed and well separated from higher states (e.g. Refs. 28,29). This excitation couples to several vibrations of the carbon backbone,[30] but the most strongly coupled modes are almost degenerate and can be treated as one effective mode (see, e.g., Ref. 31 or Sec. V). Since the vibrational quantum in the ground and excited state is almost the same, we have a textbook example of linear exciton-phonon coupling. Furthermore, other perylene derivatives show similar molecular properties but form very different crystal structures with correspondingly different crystal spectra.[32] All recent interpretations of crystal absorption spectra[24–27] use the framework of small-radius excitons. However, there is no general agreement yet about the role of CT excitons, about the choice between a complete Holstein model or a molecular vibron model, and about the concrete values of various interaction parameters.

Although motivated by perylene spectra, we will discuss general aspects of relaxed excited states in the Holstein model. This familiar one-dimensional model, as summarized in Sec. II A, has harmonic potentials with quanta $\hbar\omega$, linear electron-phonon coupling g for each molecule, and an excitation transfer integral J between neighbors. Taking g and J in units of $\hbar\omega$, we have two control parameters that encompass many cases of interest.

In the molecular limit (no interaction, $J=0$), optical absorption creates only exciton-phonon configurations at the same site. For finite J, these joint configurations can mix with configurations in which the exciton and phonons occupy different sites. The resulting eigenstates have a complex structure consisting of an exciton surrounded by a phonon cloud. We focus below on the structure and modeling of these phonon clouds.

The eigenstate structure varies widely with respect to g and J. For optical spectroscopy, the analysis typically starts with vibronic properties of isolated molecules and then introduces electronic coupling. The limiting cases are called weak (electronic) coupling and strong (electronic) coupling. This classification was introduced by Simpson and Peterson[33] and is mainly used in spectroscopy (e.g., Ref. 34). In the weak coupling regime ($J \ll g$), the transfer of electronic excitation is "slow" compared to the nuclear relaxation time within the molecule. The crystal spectrum will then resemble the vibronic structure of the isolated molecule. In the strong coupling regime ($J \gg g$), the electronic transfer is "fast" compared to the nuclear relaxation and a Born-Oppenheimer separation between the electronic and vibronic wave functions of the whole crystal can be made. Since the

 ©2002 The American Physical Society

electronic excitation is now completely delocalized, the coupling to the vibrational system vanishes and the spectrum becomes a single narrow line. We adopt the spectroscopic classification of the limiting cases and consider weak to intermediate coupling.

In the context of charge-carrier mobilities, by contrast, the natural starting point is delocalized electronic excitations. The coupling to vibrational modes of the lattice is then introduced as the second step. From this point of view, the relevant limiting cases are classified in the opposite spirit: There is either "weak (electron-phonon) coupling" ($g \ll J$) or "strong (electron-phonon) coupling" ($g \gg J$).

The Holstein Hamiltonian has been extensively studied and reviewed in the context of mobility at zero and finite temperatures.[17,18,35–41] Since the Hamiltonian cannot be solved analytically, the emphasis in these traditional works lies on studies of perturbative limits. In the course of renewed interest in molecular crystals and other narrow-bandwidth systems and in connection with increasing computer capabilities, a variety of numerical studies have recently been undertaken to explore the lowest state in the full parameter range. These include variational approaches,[42–48] direct diagonalization,[49–53] quantum Monte Carlo calculations[54–57] and density-matrix renormalization-group techniques.[58]

Compared to this, the properties of higher states have been much less investigated. These excited vibronic states, however, are essential for an understanding of optical absorption spectra. The relevant issues were identified in the initial studies of molecular crystals and limiting cases were analyzed (see, e.g., Refs. 34, 59). For intermediate coupling, however, only a few quantitative studies have been published. These include direct diagonalization studies of dimers,[60,24] variational and direct-diagonalization study of linear aggregates,[61–64] and a discussion of the second lowest vibronic state in an infinite chain.[53]

In this article, we describe a direct-diagonalization approach to the complete optical spectrum of vibronic states. For direct diagonalization, the choice of a proper basis set is crucial to allow convergence and sufficient flexibility without becoming inconveniently large. We consider an infinite chain and include translational symmetry by using basis states in momentum space. Thus, some of the finite-size issues in aggregate studies are avoided from the outset. The truncation of the basis set is done by considering only phonon clouds localized around the exciton. Furthermore, we use a displaced oscillator basis (Lang-Firsov basis), which is exact for the molecular limit of no hopping. This scheme allows a flexible description of weak and intermediate electronic coupling ($g \approx 1$, $|J| \lesssim 1$). In this regime, optical spectra can be calculated with an accuracy sufficient for comparison with experiments by diagonalizing matrices of dimension $\lesssim 5000$. Thus, standard eigenvalue routines can be used and the nature of all excited states can easily be investigated. Our approach is extended to include charge-transfer states. Applications to absorption spectra of PTCDA and MePTCDI are given as examples.

II. THE FRENKEL PROBLEM: REPRESENTATION AND SCHEME FOR NUMERICAL SOLUTION

A. The Holstein Hamiltonian

The Holstein model[17,18] assumes a one-dimensional molecular chain. Each molecule has one vibrational and one electronic degree of freedom. Vibrationally, each molecule n has one effective configuration coordinate λ_n. The vibrational potential is $V_n^{\mathrm{gr}} = \lambda_n^2$ in the electronic ground and $V_n^{\mathrm{ex}} = (\lambda_n - g)^2$ in the excited state. All energies are measured in units of the vibrational quantum $\hbar\omega$. The dimensionless exciton-phonon coupling constant g is related to the vibrational relaxation energy (Franck-Condon energy) of the excited molecule by $E_{\mathrm{FC}} = g^2$. Creation and annihilation operators for vibrations in the potential V_n^{gr} are denoted by $b_n^\dagger$ and b_n.

Electronically, molecule n can be either in the ground state or in the first excited state. Operators $a_n^\dagger$ are introduced to create an excitation at site n from the electronic ground state of the chain $|0^{\mathrm{el}}\rangle$. In the Holstein model, the quasiparticle $a_n^\dagger|0^{\mathrm{el}}\rangle$ can be either an exciton or, as originally discussed, a charge carrier. The hopping integral J (in units of $\hbar\omega$) describes the nearest-neighbor transfer of the quasiparticle as in a tight-binding model.

Using these definitions, the complete Holstein Hamiltonian for a Frenkel exciton (FE) can be written as

$$H_{\mathrm{hol}}^{\mathrm{FE}} = H_{\mathrm{elec}}^{\mathrm{FE}} + H^{\mathrm{ph}} + H^{\mathrm{FE\text{-}ph}}, \tag{1}$$

$$H_{\mathrm{elec}}^{\mathrm{FE}} = J \sum_n \left(a_n^\dagger a_{n+1} + a_{n+1}^\dagger a_n\right), \tag{2}$$

$$H^{\mathrm{ph}} = \sum_n b_n^\dagger b_n, \tag{3}$$

$$H^{\mathrm{FE\text{-}ph}} = \sum_n a_n^\dagger a_n \left[-g\left(b_n^\dagger + b_n\right) + g^2\right]. \tag{4}$$

Here, the last term $H^{\mathrm{FE\text{-}ph}}$ couples linearly the otherwise independent exciton and phonon systems. Thus, the Holstein Hamiltonian operates on states that generally consist of both exciton and phonon excitations. Such states, if they contain at least one exciton, are called vibronic states.

The Holstein Hamiltonian conserves the number of excitons. We are interested only in the states with exactly one exciton. Therefore, Eqs. (1)–(4) are already written for this subspace of "one-exciton states," and the exciton counting term $\Sigma_n a_n^\dagger a_n$ is omitted. The constant g^2 in Eq. (4) is added to align the zero of the energy axis with the lowest vibronic state of the molecular limit ($J = 0$). This energy scale reflects the exciton viewpoint, in which the states of the isolated molecules including their internal exciton-phonon coupling are used as reference states. The lowest vibronic state from our one-exciton space should not be confused with the total ground state of the crystal, in which there are neither exciton nor phonon excitations.

B. Basis set and matrix elements

Our aim is to find numerically the low energy eigenstates of the Holstein Hamiltonian (1) within the one-exciton manifold. As basis functions, we use the eigenstates $|n\underline{\nu}\rangle$ from the limiting case of zero exciton hopping ($J=0$). We call this the molecular limit, since all intermolecular interaction terms are turned off now. In the molecular limit, an exciton localized at site n is stationary and the vibrational wave functions at this site are given by oscillator functions in the displaced potential V^{ex}. At all other sites, which we count relative to the position of the exciton, the vibrational wave functions are oscillator functions in the ground state potential V^{gr}.

Thus, the basis functions can be written as

$$|n\underline{\nu}\rangle \equiv |n\rangle|\cdots\nu_{-1}\tilde{\nu}_0\nu_1\cdots\rangle \tag{5}$$

$$\equiv \underbrace{a_n^\dagger|0^{\mathrm{el}}\rangle}_{\text{elec}} \times \underbrace{\frac{1}{\sqrt{\nu_0!}}(\tilde{b}_n^\dagger)^{\nu_0}|\tilde{0}_n\rangle}_{\text{displaced on } n}$$

$$\times \underbrace{\prod_{m\neq 0}\frac{1}{\sqrt{\nu_m!}}(b_{n+m}^\dagger)^{\nu_m}|0_{n+m}\rangle}_{\text{undisplaced otherwise}}. \tag{6}$$

Here, the first factor (''electronic'') describes the electronic part of a localized Frenkel exciton at site n. The second factor (''displaced'') describes internal phonons at this site n of the exciton. The displaced ground state is denoted by $|\tilde{0}_n\rangle$ and the operator $\tilde{b}_n^\dagger = b_n^\dagger - g$ creates phonon excitations in this potential. The third factor (''undisplaced'') describes internal phonons at all sites different from n in the undisplaced potential. The choice of the displaced basis functions from Eq. (5) corresponds to applying the polaron canonical transformation (Lang-Firsov transformation) to a set of basis functions, in which all vibrational functions (including the site n of the exciton) are oscillator functions in the ground state potential (Ref. 35 or see, e.g., Ref. 39, p. 98, Ref. 40, p. 25).

The phonon-cloud state $|\underline{\nu}\rangle$ contains the phonon occupation numbers ν_m around the exciton for all lattice sites. In long notation $|\cdots\nu_{-1}\tilde{\nu}_0\nu_1\cdots\rangle$, the special position of the exciton ($m=0$) is denoted by a tilde. A complete phonon-cloud basis for a chain of N molecules consists of N-boson states and leads to huge basis sets even for small occupation numbers. But a far smaller basis is sufficient to calculate the absorption spectrum. Optical absorption from the electronic and vibrational ground state only creates phonons at the site of the electronic excitation, i.e. only states of the form $|\cdots 000\tilde{\nu}_0 000\cdots\rangle$. Excited states with any $\nu_m \neq 0$ for $m \neq 0$ cannot be reached optically.

For $J=0$, these ''dark'' states cannot mix with the optically active basis states either. Then, instead of the N-particle states $|\underline{\nu}\rangle$ we can use the one-particle states $|\nu_0\rangle$. For $|J|>0$, the dark basis states can mix with the optically active states. That means that optical absorption creates a state in which phonons are excited at arbitrary distance from the exciton site. However, the contribution of such separated configurations decreases with increasing exciton-phonon separation. Thus, the exciton will be surrounded by a *localized* phonon cloud. The localized nature of phonon clouds is the motivation for our choice of basis functions. Instead of N-dimensional cloud states $|\underline{\nu}\rangle$, a finite range $|\nu_{-M}\cdots\tilde{\nu}_0\cdots\nu_M\rangle$, with M denoting the extension of the phonon cloud, will be sufficient. Numerically, M can be increased until convergence is reached.

With the restriction to local phonon clouds around the exciton, we Fourier transform the basis states (5):

$$|k\underline{\nu}\rangle \equiv \frac{1}{\sqrt{N}}\sum_n e^{ikn}|n\underline{\nu}\rangle. \tag{7}$$

These states represent an exciton ''dressed'' with a local phonon cloud. The index k gives the quasimomentum of the whole object, i.e., the dressed exciton, and k is a good quantum number due to translational symmetry. Thus, for any given k the basis set consists only of a set of phonon cloud configurations. We emphasize that in contrast to the real-space basis (5), the momentum-space basis functions (7) are not Born-Oppenheimer separable into a product of a purely electronic and a purely vibrational part.

Having specified the basis states, the Hamiltonian can be represented as a matrix. Application of $H_{\mathrm{Hol}}^{\mathrm{FE}}$ to the real space states from Eq. (5) yields the matrix elements

$$\langle m\underline{\mu}|H_{\mathrm{Hol}}^{\mathrm{FE}}|n\underline{\nu}\rangle = \delta_{m,n}\langle\underline{\mu}|\underline{\nu}\rangle\sum_i \nu_i + J\left[\delta_{m,n-1}\mathcal{F}_{-1}\begin{pmatrix}\underline{\mu}\\ \underline{\nu}\end{pmatrix} + \delta_{m,n+1}\mathcal{F}_{+1}\begin{pmatrix}\underline{\mu}\\ \underline{\nu}\end{pmatrix}\right]. \tag{8}$$

The first term in this compact notation results from the operators H^{ph} and $H^{\mathrm{FE\text{-}ph}}$. They contain no interactions between different sites and thus simply count the phonons in the Lang-Firsov basis. The overlap factor $\langle\underline{\mu}|\underline{\nu}\rangle$ stands for the total overlap of two phonon clouds centered at the same lattice site. It is nonzero only for identical clouds due to the orthogonality of the oscillator functions

$$\langle\underline{\mu}|\underline{\nu}\rangle = \prod_i \langle\mu_i|\nu_i\rangle, \tag{9}$$

where $\langle\mu|\nu\rangle = \delta_{\mu\nu}$ is the overlap between oscillator functions in the same potential.

The second term in Eq. (8) results from the purely electronic Frenkel transfer process $H_{\mathrm{elec}}^{\mathrm{FE}}$. The vibrational part of the basis functions factors out and leads to the Franck-Condon overlaps $\mathcal{F}_{\pm 1}$ for the total vibronic overlap of the phonon cloud $\underline{\nu}$ centered at n and the phonon cloud $\underline{\mu}$ centered at $m=n\pm 1$:

$$\mathcal{F}_{-1} = S\begin{pmatrix}\mu_0\\ \nu_{-1}\end{pmatrix}S\begin{pmatrix}\nu_0\\ \mu_{+1}\end{pmatrix}\prod_{i\neq 0,1}\langle\mu_i|\nu_{i-1}\rangle, \tag{10}$$

$$\mathcal{F}_{+1}=S\begin{pmatrix}\nu_0\\ \mu_{-1}\end{pmatrix}S\begin{pmatrix}\mu_0\\ \nu_{+1}\end{pmatrix}\prod_{i\neq -1,0}\langle\mu_i|\nu_{i+1}\rangle. \tag{11}$$

Here, $S\binom{\nu}{\mu}$ is the overlap between a displaced oscillator function with quantum number ν and an undisplaced function with quantum number μ (Ref. 65)

$$S\begin{pmatrix}\nu\\ \mu\end{pmatrix}\equiv\left\langle\frac{1}{\sqrt{\mu!}}(b^\dagger)^\mu 0\middle|\frac{1}{\sqrt{\nu!}}(\tilde{b}^\dagger)^\nu 0\right\rangle$$
$$=\frac{e^{-g^2/2}}{\sqrt{\mu!\,\nu!}}\sum_{i=0}^{\min(\mu,\nu)}\frac{(-1)^{\nu-i}g^{\mu+\nu-2i}\mu!\,\nu!}{i!(\mu-i)!(\nu-i)!}. \tag{12}$$

It is obvious that in the Lang-Firsov basis the strength g of the exciton-phonon coupling enters only through the magnitude of the factors $\mathcal{F}_{\pm 1}$ in the intersite hopping term.

In the momentum space representation (6), the Hamiltonian matrix becomes

$$\langle k\underline{\mu}|H^{\mathrm{FE}}_{\mathrm{Hol}}|k\underline{\nu}\rangle=\langle\underline{\mu}|\underline{\nu}\rangle\sum_i\ \nu_i$$
$$+J\left[e^{-ik}\mathcal{F}_{-1}\begin{pmatrix}\underline{\mu}\\ \underline{\nu}\end{pmatrix}+e^{+ik}\mathcal{F}_{+1}\begin{pmatrix}\underline{\mu}\\ \underline{\nu}\end{pmatrix}\right]. \tag{13}$$

For general momenta k, these matrix elements are complex numbers. For our intended application to spectroscopy, the values at the Brillouin-zone edges ($k=0,\pi$) are of interest and there the matrix elements are real. Representing the final eigenstates as

$$|\Psi_j(k)\rangle=\sum_{\underline{\nu}}\ u_{\underline{\nu}j}(k)|k\underline{\nu}\rangle, \tag{14}$$

we obtain the eigenvalue problem

$$\sum_{\underline{\mu}}\ \langle k\underline{\mu}|H^{\mathrm{FE}}_{\mathrm{Hol}}|k\underline{\nu}\rangle u_{\underline{\mu}j}=E_j u_{\underline{\nu}j} \tag{15}$$

for the real matrix $\langle k\underline{\mu}|H^{\mathrm{FE}}_{\mathrm{Hol}}|k\underline{\nu}\rangle$. Its eigenvalues E_j and eigenstates $|\Psi_j(k)\rangle$ are the stationary solutions of the Holstein Hamiltonian (1).

C. Transition dipoles and phonon clouds of the eigenstates

The properties of the eigenstates (14) are easily computed. We start with the transition dipole moment between the eigenstates and the total ground state. For a light wave with wave vector q, the transition dipole operator is

$$\hat{P}_q=\frac{1}{\sqrt{N}}\sum_n\ e^{-iqn}(a_n^\dagger+a_n), \tag{16}$$

The normalization is such that the absolute squared transition dipole per unit cell becomes $\vec{p}_M^{\,2}$, with $\vec{p}_M$ being the molecular transition dipole. The transition dipole of a state $|\Psi_j(k)\rangle$ will be nonzero only for $q=k$. Therefore, we introduce a k-dependent transition dipole

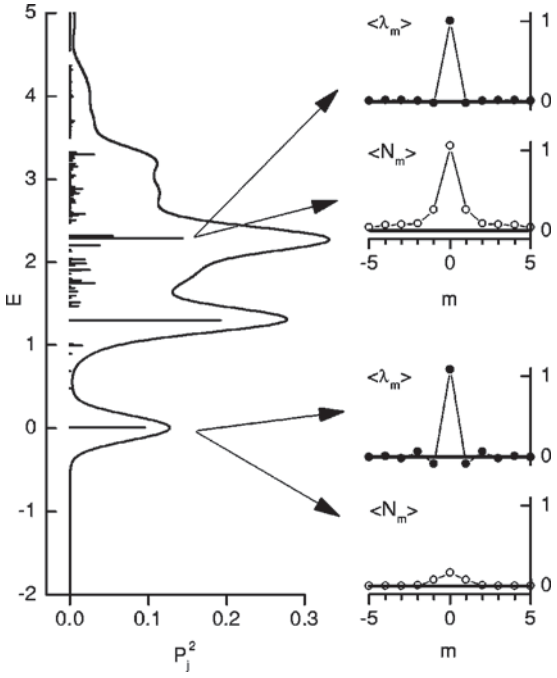

FIG. 1. Illustration of the eigenstates and their properties for a numerical solution of the Holstein model (1) with parameters $J=0.5$ and $g=1$ at total momentum $k=0$. In the left panel, the optically active eigenstates are shown at a vertical energy axis. The sticks indicate the spectral weight P_j^2 of each state according to Eq. (17). For a visualization of the resulting spectrum, the stick spectrum is convolved with a Gaussian (standard derivation $\sigma=0.15$) and the broadened spectrum is scaled for easy superposition [here, area $\int f(E)dE=0.5$]. In the right panels, the occupation number clouds $\langle\hat{N}_m\rangle$ and displacement clouds $\langle\hat{\lambda}_m\rangle$ are shown for two particular eigenstates [see comments to Eqs. (20) and (21)].

$$P_j(k)\equiv\langle\Psi_j(k)|\hat{P}_k|0^{\mathrm{tot}}\rangle. \tag{17}$$

Inserting the explicit expression (13), one obtains

$$P_j(k)=\sum_{\underline{\nu}}\ u^*_{\underline{\nu}j}S\begin{pmatrix}\nu_0\\ 0\end{pmatrix}\prod_{r\neq 0}\langle\nu_r|0\rangle. \tag{18}$$

The squares of these transition moments are the spectral weights of the corresponding states and obey the sum rule

$$\sum_j\ P_j^2(k)=1. \tag{19}$$

For $k=0$, $P_j(0)$ gives the transition dipole for optical excitation, and $P_j^2(0)$ determines the spectral weight of the state in an absorption spectrum. For general k, the spectral weight $P_j^2(k)$ can be viewed as the exciton character of state $|\Psi_j(k)\rangle$ since $P_j(k)$ is the projection of this state onto a Frenkel exciton without phonon excitations.

As an illustration, we show in Fig. 1 the results of such a calculation for $k=0$ and the parameters $J=0.5$ and $g=1$. The energy levels E_j of the eigenstates are arranged at a vertical energy axis in the left part. Their spectral weight P_j^2 is indicated by the horizontal length of each stick. The lowest state appears as a solitary stick at $E_1=0.0074$. At higher

energies, the spectrum consists of many densely packed lines resulting from the mixture of the various phonon cloud configurations in the basis set. The numerical spectrum remains discrete only because the basis is finite. To illustrate the dense vibronic manifold, we always convolve stick spectra with a Gaussian of constant standard derivation ($\sigma = 0.15$) and show the broadened spectrum using a convenient scaling factor.

Another important property of a vibronic state $|\Psi_j(k)\rangle$ is the internal structure of its phonon cloud. One measure to characterize it is the set of expectation values $\langle \hat{N}_m \rangle$ for the occupation number operators

$$\langle \hat{N}_m \rangle \equiv \left\langle \sum_n a_n^\dagger a_n b_{n+m}^\dagger b_{n+m} \right\rangle. \tag{20}$$

These occupation numbers show how many phonons are excited at the oscillator that is m lattice spacings from the exciton. Note that they depend on the displacement chosen for the oscillator functions in the basis set. Thus, they are no observable quantities. They are mainly important for choosing a reasonable basis set: Since numerically for each relative site m, only states up to a predefined number $\nu_m^{\max}$ can be included in the basis set, it must be assured that $\langle \hat{N}_m \rangle \ll \nu_m^{\max}$. These phonon occupation numbers are again illustrated in Fig. 1 for two representative eigenstates of high spectral weight. For the lowest state at $E_1 = 0.0074$, there are 0.16 phonons at the exciton site ($m = 0$), and the total phonon number is $\Sigma_m \langle N_m \rangle = 0.34$. In the molecular limit, this state would be the zero-phonon state, but the hopping term J leads to a nonzero phonon occupation number. At a higher state $E_{41} = 2.28$, the total phonon number is 2.12 with a peak value of $\langle \hat{N}_0 \rangle = 1.05$. This state originates from the two-phonon state in the molecular limit. Electronic delocalization leads to broad phonon clouds.

A description of the phonon cloud that is independent of the basis set can be provided by the expectation values of the displacement operators

$$\langle \hat{\lambda}_m \rangle \equiv \left\langle \sum_n a_n^\dagger a_n \frac{b_{n+m}^\dagger + b_{n+m}}{2} \right\rangle. \tag{21}$$

This displacement cloud $\langle \lambda_m \rangle$ gives the average distortion from equilibrium (along the dimensionless normal coordinate λ) at a molecule which is m sites from the exciton. Note that the exciton itself is completely delocalized in real space and so is the displacement cloud. With respect to the basis representation (5), the displacement cloud of a state $|\Psi_j(k)\rangle$ (14) is obtained as

$$\langle \hat{\lambda}_m \rangle = \sum_{\underline{\mu}\,\underline{\nu}} u_{\underline{\mu}j}^* u_{\underline{\nu}j} \times \left(\prod_{r \neq m} \langle \mu_r | \nu_r \rangle \right) \left(\frac{\sqrt{\nu_m + 1}}{2} \langle \mu_m | \nu_m + 1 \rangle + \frac{\sqrt{\nu_m}}{2} \langle \mu_m | \nu_m - 1 \rangle + g\, \delta_{m,0} \langle \mu_0 | \nu_0 \rangle \right). \tag{22}$$

Again, Fig. 1 may serve as an illustration. There, the displacement clouds are shown for the same representative states that were analyzed in terms of occupation number clouds. The narrow clouds show that the actual lattice distortion is much more localized around the exciton than the broad occupation number clouds might suggest. This difference results from the fact that the vibronic wave function in the actual eigenstates cannot be accurately represented by single oscillator functions of the special Lang-Firsov basis.

D. Truncated phonon basis and symmetry adaptation

By now, the formal tools for calculating and analyzing the eigenstates of the Holstein Hamiltonian (1) have been collected. The only remaining issue is how to truncate the infinite phonon-cloud basis to a number that allows numerical diagonalization. For this, we first restrict the basis to cloud states of the form

$$|\underline{\nu}_M\rangle = |\nu_{-M} \cdots \tilde{\nu}_0 \cdots \nu_{+M}\rangle. \tag{23}$$

This means that only phonon clouds localized at the $2M+1$ molecules around the exciton are included whereas free phonons can only be approximated using large M.

Second, for each position in the phonon-cloud we restrict the maximum occupation number

$$\nu_m \leqslant \nu_m^{\max}. \tag{24}$$

In this way, the localized nature of the phonon cloud can better be taken into account by considering only small occupation numbers $\nu_m^{\max}$ at sites far away from the exciton. A typical cutoff vector as used for the calculation in Fig. 1 has $M = 5$ and $|\underline{\nu}^{\max}\rangle = |12345\tilde{6}54321\rangle$.

Third, among these states we include only those for which the total number of phonons does not exceed a given maximum

$$\sum_m \nu_m \leqslant \nu_{\text{tot}}^{\max}. \tag{25}$$

In this way, high-energy basis states are excluded. Since the overlap factors for states with high vibrational excitation decrease rapidly, these states do not appear in the absorption spectrum. Condition (24) is only effective for $\nu_{\text{tot}}^{\max} < \Sigma_m \nu_m^{\max}$, but typically it can be used as a strong restriction (e.g., $\nu_{\text{tot}}^{\max} = 6$ in Fig. 1).

Now, we have arrived at a fairly complex description for the cut-off conditions of the basis set, given by the numbers M, $\underline{\nu}^{\max}$, $\nu_{\text{tot}}^{\max}$. However, this complex scheme allows to choose a basis just large enough to represent the optically active eigenstates of the Hamiltonian.

The minimum radius $M = 0$ is an important special case of the phonon basis in which electronic and vibrational excitations are always at the same site, just as in the $J = 0$ limit. These joint exciton-phonon configurations can be considered as distinct molecular excited states and treated within the standard framework of Frenkel exciton theory. Following Broude, Rashba, and Sheka (Ref. 66, p. 185), we call this the molecular vibron model:

$$M = 0. \tag{26}$$

The molecular vibron model follows naturally from the exciton concept and was successfully applied to early interpretations of crystal spectra.[67] The approximation is additionally justified if—beyond the simplest Holstein Hamiltonian (1)—the phonon energy differs between the electronic ground and excited state of the molecule (see Ref. 34, p. 87ff or Ref. 66, p. 198f).

To find a suitable phonon basis for concrete calculations, we start with the molecular vibron model and gradually increase the phonon basis until the obtained absorption spectrum converges. This procedure is demonstrated in Sec. (III).

In addition to the general truncation scheme, in some cases the dimension of the phonon basis can be reduced by symmetry. For the Frenkel exciton problem in this section, we have inversion symmetry about the exciton's site. So we can introduce symmetry adapted basis states $|k\underline{\nu}\rangle_{\pm}$ in which the phonon cloud is either symmetric $(+)$ or antisymmetric $(-)$ with respect to inversion about its center. Inversion of the phonon cloud in the nonadapted basis (7) shall be denoted by an overbar:

$$|\overline{\underline{\nu}}\rangle: \quad \overline{\nu}_n = \nu_{-n}. \tag{27}$$

Even the nonadapted basis contains some symmetric phononclouds ($\overline{\underline{\nu}}=\underline{\nu}$). For all other states, a symmetry adaption has to be chosen. Thus, the symmetry adapted states can be obtained as

$$|k\underline{\nu}\rangle_{+} = \begin{cases} |k\underline{\nu}\rangle & \text{for} \quad \overline{\underline{\nu}}=\underline{\nu}, \\ \frac{1}{\sqrt{2}}(|k\underline{\nu}\rangle + |k\overline{\underline{\nu}}\rangle) & \text{for} \quad \overline{\underline{\nu}}\neq\underline{\nu}, \end{cases}$$

$$|k\underline{\nu}\rangle_{-} = \frac{1}{\sqrt{2}}(|k\underline{\nu}\rangle - |k\overline{\underline{\nu}}\rangle) \quad \text{for} \quad \overline{\underline{\nu}}\neq\underline{\nu}. \tag{28}$$

Now, the symmetric subspace spanned by the $|k\underline{\nu}\rangle_{+}$ states does not mix with the antisymmetric subspace spanned by the $|k\underline{\nu}\rangle_{-}$ states and the diagonalization can be done separately for both subspaces. For a large cutoff radius of the phonon cloud, the dimension of the two subspaces is roughly one half of the original basis. Furthermore, the transition dipoles of all antisymmetric states vanish exactly and only the symmetric space is needed for the absorption spectrum.

III. FRENKEL EXCITON SPECTRA

A. Overview

The Holstein Hamiltonian (1) contains two parameters: The exciton hopping integral J and the exciton-phonon coupling constant g. Both are already scaled in units of the third physical parameter of the system: the vibrational quantum $\hbar\omega$. Thus, the parameter space cannot be reduced to less than two dimensions anymore. The qualitative character of the solutions strongly depends in a complicated way on both control parameters. We will explore only a certain region of this parameter space.

In Sec. III B, the molecular limit ($J=0$) and the case of weak electronic coupling ($J \ll g$) is considered. The zero-phonon and the one-phonon space will be analyzed for arbitrary g using perturbation theory. This analysis illustrates what type of phonon basis is needed in various situations.

In Sec. III C, numerical solutions will be presented for some intermediate coupling situations ($J=0.5$ and $J=1$). This coupling range is considered only for $g=1$ since in the intended applications g typically is in this order.

B. Perturbative limit for weak coupling

One extreme case is the molecular limit $J=0$. In this case, all basis states (7) are eigenstates and the molecular vibron model ($M=0$) is sufficient to describe the optically active states. The spectrum is the nondispersive vibronic progression of an isolated molecule:

$$E_j^{(0)}(k) = \nu, \quad \nu(j) = j-1 = 0,1,2,\ldots, \tag{29}$$

$$P_j^2(k) = S^2\begin{pmatrix} \nu \\ 0 \end{pmatrix} = \frac{g^{2\nu}}{\nu!}e^{-g^2}, \tag{30}$$

For $g=1$, the lowest and second lowest state have equal spectral weight ($P_1^2=P_2^2$) and the weight of higher states decreases rapidly. The displacement cloud is strictly localized at the site of the exciton

$$\langle \lambda_m \rangle = g\,\delta_{m,0}. \tag{31}$$

For finite $J \ll g$, one can start with the molecular limit and apply first order perturbation theory in the parameter J. The lowest state of the unperturbed system is $|k\underline{\nu}\rangle$ with $|\underline{\nu}\rangle = |\cdots 0\tilde{0}0\cdots\rangle$. This state at $E_1^{(0)}=0$ is nondegenerate, and application of first order perturbation theory gives immediately

$$E_1^{(1)} = 2J\cos(k)S^2\begin{pmatrix} 0 \\ 0 \end{pmatrix} = 2J\cos(k)e^{-g^2}. \tag{32}$$

This result is well known from small polaron theory for zero temperature. The width $4J$ of the purely electronic band is renormalized by the overlap factor e^{-g^2} since the exciton moves together with its displacement cloud.

Little attention has been paid, however, to the fate of higher vibronic states under the effect of the small perturbation J. Let us consider the one-phonon states in more detail.

In the molecular limit, the only optically active one-phonon state has the cloud $|\underline{\nu}\rangle = |\cdots 000\tilde{1}000\cdots\rangle$ with one on-site phonon. This state is degenerate with all other dark basis states that contain one phonon excitation at an arbitrary exciton-phonon separation n. A perturbation $J>0$ will mix all these states and lift their degeneracy. This can be analyzed by writing down the matrix elements (13) for the states of the one-phonon manifold. The phonon cloud of the state $|k\underline{\nu}(n)\rangle$ has the structure $\nu_i=\delta_{i,n}$ and analogously for $|k\underline{\mu}(m)\rangle$: $\mu_i=\delta_{i,m}$. The matrix representation (13) then becomes

$$H_{mn} = \langle k\underline{\mu}(m)|H_{\mathrm{Hol}}^{\mathrm{FE}}|k\underline{\nu}(n)\rangle = \delta_{m,n} + Je^{-g^2}(W_{mn}+g^2V_{mn}), \tag{33}$$

where

$$W_{mn}=\delta_{m,n+1}\cdot e^{-ik}+\delta_{m,n-1}\cdot e^{+ik}, \tag{34}$$

and V_{mn} is a matrix that has nonzero elements only for $|m|,|n|\leqslant 1$. That means, V_{mn} only mixes the states where the phonon is located either at the exciton site or at its nearest neighbor.

The two contributions W_{mn} and V_{mn} in the nondiagonal perturbation term of Eq. (32) act in completely different ways. Let us first discuss the case of $g\ll 1$ and neglect V_{mn}. For $k=0$ or $k=\pi$, W_{mn} is the Hamiltonian of a nearest-neighbor hopping particle on an infinite chain with open boundary. This gives a wavelike solution. In contrast to the ordinary hopping problem, the exact consideration of the specific boundary conditions is essential now. Only then, the correct amplitude at the special site $n=0$ can be obtained; and this amplitude alone determines the spectral weight. Thus, one obtains the eigenstates

$$|\Psi_j\rangle=\frac{1}{\sqrt{M+1}}\sum_{n=-M}^{M}\sin\left(\frac{nj\pi}{2M+2}\right)|k\underline{\nu}(n)\rangle \tag{35}$$

with

$$j=1,2,\ldots,2M+1. \tag{36}$$

Their energies are

$$E_j^{(1\mathrm{ph},g\ll 1)}=1\pm 2Je^{-g^2}\cos\left(\frac{j\pi}{M+1}\right), \tag{37}$$

where $\pm$ refers to $k=0$ and $k=\pi$, respectively. The spectral weight of state j at $k=0$ follows from definition (17). It has only two values depending on the index j:

$$P_j^2=\begin{cases}\dfrac{1}{M+1}g^2e^{-g^2} & \text{for odd} \quad j,\\ 0 & \text{for even} \quad j.\end{cases} \tag{38}$$

The M states with even j and zero spectral weight belong to the subspace of the antisymmetric states in the symmetry adapted basis (28). The $M+1$ optically active states with odd j are the symmetric states. These active states form a band of equally absorbing states with a total width of $4Je^{-g^2}$. The total spectral weight of these active states sums up to $g^2e^{-g^2}$ representing the value of the molecular limit. In all these states, the phonon cloud is not localized around the exciton but consists of a standing phonon wave. We emphasize that this behavior is the limit for small g. In this limit, the total spectral weight of the considered one-phonon band is only a small feature in the overall spectrum since the major part of the spectral weight is concentrated in the zero-phonon state.

Complementary, the V_{mn} part in the perturbation (33) mixes only the cloud states with phonon excitations at or next to the exciton site. Therefore, in the limit of large g, the basis set can be reduced to include only local phonon cloud configurations up to the nearest neighbor ($M=1$). Using the symmetry adapted basis functions (28), the symmetric one-phonon subspace consists only of two phonon configurations $|\Phi_1(k)\rangle=|k\rangle|0\tilde{1}0\rangle_+$ and $|\Phi_2(k)\rangle=|k\rangle|1\tilde{0}0\rangle_+$. The Hamiltonian in the representation of these two states takes the form

$$H_{mn}=\delta_{mn}+2Je^{-g^2}\cos(k)\begin{pmatrix} g^2 & \dfrac{1-g^2}{\sqrt{2}} \\ \dfrac{1-g^2}{\sqrt{2}} & \dfrac{1}{2}g^2 \end{pmatrix} \tag{39}$$

with eigenvalues

$$E_\pm^{(1\mathrm{ph},g\gg 1)}=1+2J\cos(k)g^2e^{-g^2}\times\frac{3}{4}\left(1\pm\sqrt{1-\frac{16}{9g^2}+\frac{8}{9g^4}}\right). \tag{40}$$

Thus, the zero-order energy $E=1$ splits into two bands $E_\pm(k)$. Similarly to the perturbation-in-J treatment of the lowest state (32), the electronic bandwidth $4J$ is multiplied by an overlap factor $g^2e^{-g^2}$ which corresponds to the interaction of the transition-dipole moments of the molecular one-phonon state. However, there are *two* states now. In the limit $g\to\infty$, their energies tend to

$$E_+^{(1\mathrm{ph},g\to\infty)}\to 1+2J\cos(k)g^2e^{-g^2}\times\frac{3}{4}, \tag{41}$$

$$E_-^{(1\mathrm{ph},g\to\infty)}\to 1. \tag{42}$$

In this limit, both states still have spectral weights of $P_+^2\to\frac{2}{3}$ and $P_-^2\to\frac{1}{3}$.

This splitting into two states which both carry spectral weight is entirely caused by the delocalization of the phonon cloud. Such a delocalization is neglected in the simplest approach of the molecular vibron model (26), which would mean the neglect of state $|\Phi_2(k)\rangle$ in Hamiltonian (39). Looking at the nondiagonal term in Hamiltonian (39) suggests, and closer inspection of the full one-phonon subspace Hamiltonian (33) confirms: For the special value $g=1$, the molecular vibron state $|k\underline{\nu}(n=0)\rangle$ decouples from all other phonon cloud configurations. Only in this case, the molecular vibron model becomes exact (in the one-phonon subspace) and yields one energy band at

$$E^{(1\mathrm{ph},g=1)}=1+2J\cos(k)g^2e^{-g^2} \tag{43}$$

which carries all the spectral weight $g^2e^{-g^2}$.

To give an illustration of the phenomena in the one-phonon subspace and to show the relevance of the described limiting cases, we show a numerical solution in Fig. 2. For this, we solved the Hamiltonian (32) numerically for a phonon cloud of radius $M=20$ at the total momentum $k=0$. For $k=\pi$, the spectra only have to be mirrored with respect to $E=1$.

In Fig. 2(a), the "exact" numerical results (graph 1) are shown for a relatively small $g=0.5$. The tendency of a broad band with constant spectral weight is clearly visible. This bandwidth is compared to the width the free phonon part W_{mn} from Eq. (37) in graph 2. Both agree very well. The

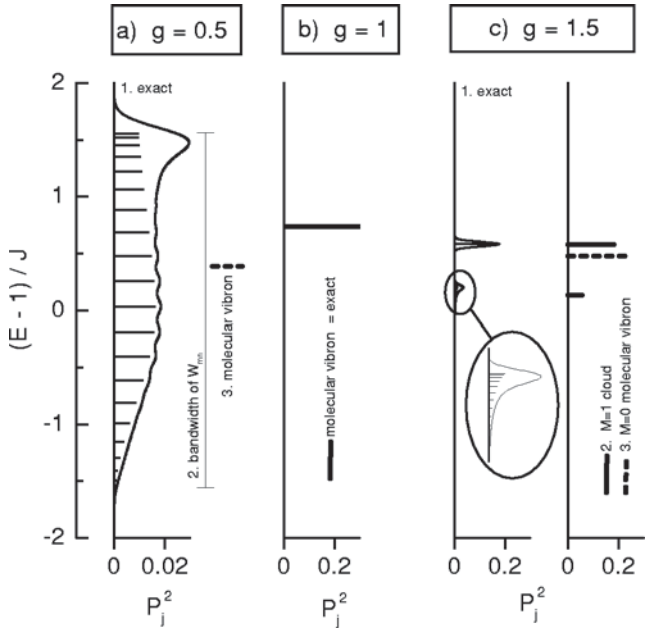

FIG. 2. Perturbative treatment $J\rightarrow 0$ of the one-phonon subspace for three coupling parameters g. The "exact" stick spectra are numerical solutions of the one-phonon Hamiltonian (33) for a phonon-cloud radius of $M=20$. The envelopes are convolutions of the stick spectra with Gaussians of appropriate width. Figure 2(a) represents the small-g case, where a broad one-phonon sideband is formed. The "exact" solution in graph 1 is compared to the bandwidth of the free-phonon part [W_{mn} from Eq. (37)] in graph 2 and to the position of the single active state from the molecular vibron model (26) in graph 3. Figure 2(b) represents the $g=1$ case, where the molecular vibron model becomes exact. Figure 2(c) represents the large-g case, in which the exciton interacts mainly with a nearest-neighbor phonon cloud. The "exact" numerical solution in graph 1 resembles the approximate solution (39) for a nearest neighbor cloud ($M=1$) in graph 2. The single state from the molecular vibron model ($M=0$) is shown in graph 3.

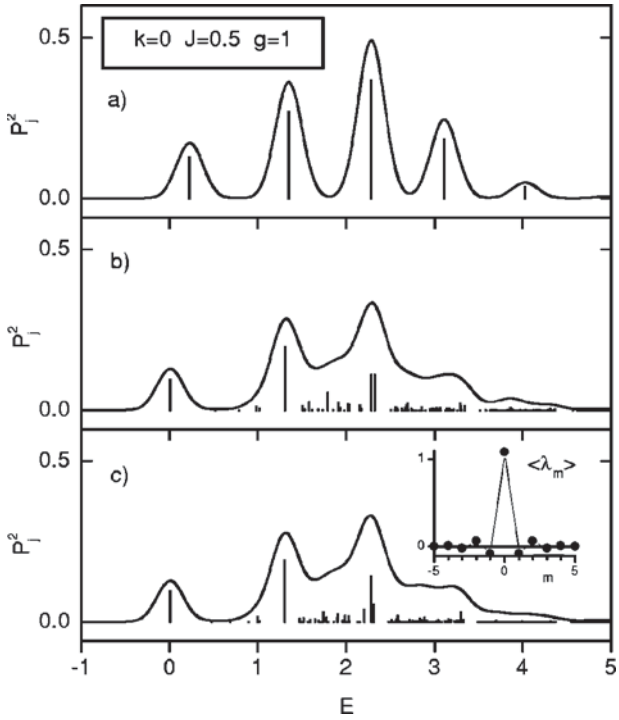

FIG. 3. Convergence of absorption spectra at the top of the band for $J=0.5$ and $g=1$ (intermediate coupling, rather small J). Panel a shows the results for the molecular vibron model (26). Panels (b) and (c) show spectra for a large phonon cloud basis. Going from (b) to (c), the maximum cloud radius M is increased from 5 to 6 and on each relative site m the maximum occupation number ν_m is increased by 1. This increases the number of symmetric basis states from 1587 in panel (b) to 4485 in c. The sticks always show the spectral weight according to Eq. (17). The solid lines are convolutions of the stick spectra with a Gaussian as in Fig. 1 (normalized to area 0.5). The shape of the thus broadened spectrum in panel c has almost converged, particulary for energies $E<2.5$. The inset in panel c shows the displacement cloud of the lowest state as in Fig. 1.

molecular vibron model ($M=0$) would give a single active state at $(E-1)/J=0.389$ (position indicated by graph 3). This state would represent the weighted center of the exact band [also at $(E-1)/J=0.389$ in this case] but it would veil the large splitting ($\Delta E/J\approx 1.55$).

In Fig. 2(b), we show the solution for $g=1$. There, the one active state of the molecular vibron model ($M=0$) is the exact solution.

In Fig. 2(c), the numerical solution is shown for a rather large $g=1.5$ (graph 1). It clearly approaches the two active states from the nearest-neighbor cloud (radius $M=1$) given by Eq. (40), which are shown in graph 2. For comparison, the result of the molecular vibron model ($M=0$) is also shown in graph 3. As for $g<1$, the molecular vibron model can only represent the weighted center of the one-phonon states but not their qualitative splitting. Note that for both cases $g<1$ and $g>1$ the correct splittings of the one-phonon states are in the same order as the perturbation parameter J.

The situation for energies above the one-phonon subspace becomes more complex and will not be considered here. Already in the two-phonon subspace, which is spanned by all zero-order basis states with a total phonon number 2, there occurs a high degeneracy of various cloud configurations. The numerical calculations in Sec. III C confirm that for not too strong electronic coupling ($J\lesssim 0.5$) and g in the order of 1, the approximation of highly localized phonon clouds or even the molecular vibron model yields a good description of the full absorption spectrum.

C. Numerical solutions for intermediate coupling

In the intermediate electronic coupling regime, the exciton hopping integral is of the order of 1. In this case, the perturbative approach from Sec. III B breaks down since, e.g., the bandwidths for the zero-phonon subspace (32) or the one-phonon subspace (40) would not be small compared to the vibronic spacing. In this case, numerical solutions using the basis from Sec. II B can be used. We will discuss the case of $g=1$, which is approximately realized for the optically coupled C-C stretching modes in many conjugated molecules (conjugated polymers, polyacenes, PTCDA derivatives).

In Fig. 3, we show the convergence for $J=0.5$ and $g=1$

at the top of the band ($k=0$). This parameter set was already used in the illustrations from Fig. 1. Figure 3(a) gives the spectrum in the molecular vibron model (25) with a maximum phonon number of $\nu_{\mathrm{tot}}^{\max}=6$. In this model, one obtains $\nu_{\mathrm{tot}}^{\max}+1$ vibronic states. Compared to the molecular limit, the molecular vibron states are shifted and their spectral weight is redistributed to higher energies due to the effect of the positive hopping integral J.

Figures 3(b) and 3(c) show the solutions for large basis sets. Only the optically active states $|k\underline{\nu}\rangle_+$ from Eqs. (28) were calculated. In both cases, $\nu_{\mathrm{tot}}^{\max}=6$ was retained as for the molecular vibron model. Only the cutoff vector $|\underline{\nu}\rangle^{\max}$ was increased from $|\underline{\nu}\rangle^{\max}=|1234\tilde{6}4321\rangle$ in Fig. 3(b) to $|\underline{\nu}\rangle^{\max}=|12345\tilde{6}54321\rangle$ in Fig. 3(c). This means that in Fig. 3(c) the cloud radius M is increased from 4 to 5 and at each cloud position the allowed number of phonons is increased by 1. This increases the number of symmetric basis states from 1587 to 4485. The broadened spectra clearly show that this increase in basis size changes the result only very little and mainly at energies $E>2.5$. The obtained accuracy is completely sufficient for interpreting experimental absorption spectra, since effects not included in the model Hamiltonian will be larger anyway.

The properties of the lowest state and a representative high-lying state with large spectral weight were already shown in Fig. 1. The occupation number clouds $\langle\hat{N}_m\rangle$ of both states are strongly localized around the exciton site and their decay patterns justify the pattern of the cutoff vector $|\underline{\nu}\rangle^{\max}$. The occupation cloud is more localized for the high-lying state than for the lowest state. Therefore, the molecular vibron model (26) is more accurate for the high-lying state, which can be seen from the comparison of Figs. 3(a) and 3(c). The main effect of the delocalized cloud basis in the high energy region is a broadening of the spectra. The lowest state, however, moves considerably from $E_1=0.229$ in the Fig. 3(a) to $E_1=0.0074$ in the largest basis set of Fig. 3(c).

The displacement clouds $\langle\hat{\lambda}_m\rangle$ show the same delocalization tendencies. Remarkably, the displacement pattern of the lowest state alternates with distance from the exciton site. This behavior can be rationalized on the level of a variational mean-field theory (as in Ref. 36) by the competition between exciton delocalization and exciton-phonon coupling: At the top of the band, the (purely electronic) exciton hopping increases the energy of the lowest state. With inclusion of exciton-phonon coupling, the hopping term gets multiplied by a vibronic overlap factor between the oscillator at the exciton site (displacement $\langle\hat{\lambda}_0\rangle$) and the oscillator at the nearest neighbor (displacement $\langle\hat{\lambda}_1\rangle$). To lower the energy, the effective hopping, i.e., the vibronic overlap, should be decreased. This can be achieved by maximizing the difference in the displacements $\langle\hat{\lambda}_0\rangle$ and $\langle\hat{\lambda}_1\rangle$. Since the total displacement is fixed by the sum rule $\Sigma_m\langle\hat{\lambda}_m\rangle=g$ (e.g. Ref. 31), an alternating displacement pattern minimizes the energy. At the bottom of the band, the same argument demands a large effective hopping and thereby the smallest possible difference in displacements, which results in a uniformly decaying displacement cloud as shown in the following Fig. 4.

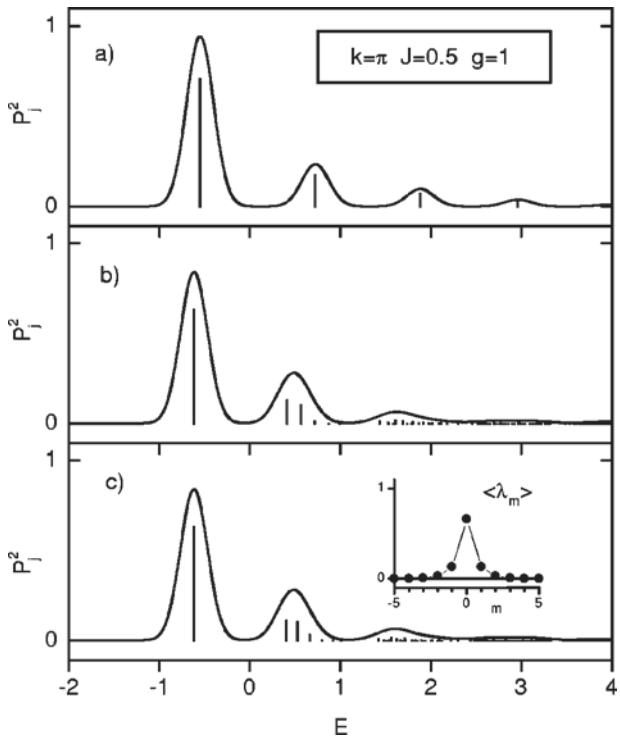

FIG. 4. Convergence of absorption spectra at the bottom of the band for $J=0.5$ and $g=1$. Panels (a), (b), and (c) show the results for the same basis sets as in Fig. 3. The broadened spectra are again normalized to area=0.5.

At the bottom of the band ($k=\pi$, Fig. 4), convergence is much easier to obtain for intermediate J. This is clear since the bottom of the band corresponds to the real ground state of the Hamiltonian, whereas the $k=0$ states at the top correspond energetically to phonon excitations of the $k=\pi$ states at lower energies. The convergence is shown for the same parameters and basis sets as at the top of the band (Fig. 3). The inset in Fig. 4(c) shows again the displacement cloud of the lowest state, which now has the nonalternating pattern as discussed in the previous paragraph.

For larger values of J, the delocalization of the phonon cloud is more pronounced and larger basis sets are needed for the same level of accuracy. In Fig. 5, we demonstrate the convergence at the top of the band for $J=1$ and the same basis sets as in Fig. 3. Now, the molecular vibron model in Fig. 5(a) deviates from the complete solution even on the energy scale of the vibronic quantum. The energy of the lowest state is overestimated by 0.88, and also the maximum of the broadened spectra deviates by almost 0.5. Even the solution in Fig. 5(b) still shows notable differences from the solution for the largest basis set in Fig. 5(c). Only the position and spectral weight of the lowest state have already converged to about two significant figures. The lowest state in panel 5(c) lies at -0.563, which reproduces two significant figures of the high-accuracy ground state calculation ($-0.5689\cdots$) reported in Ref. 53.

The convergence for $J=1$ at the bottom of the band ($k=\pi$) is shown in Fig. 6. As for $J=0.5$, the convergence is much better at the band bottom with almost no change of the broadened spectra for the basis set increase from Fig. 6(b) to

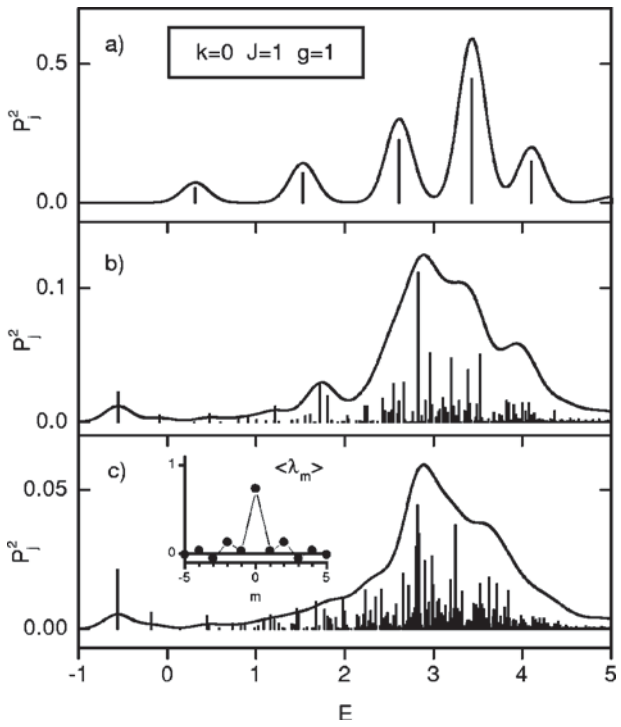

FIG. 5. Convergence of absorption spectra at the top of the band for $J=1$ and $g=1$. Panels (a), (b), and (c) show the results for the same basis sets as in Fig. 3. With increasing number of states, the spectral weight of the individual states in the higher energy region decreases. Therefore, the y-axis scaling and the normalization of the broadened spectra is different in each panel. [Area = 0.5 in panel (a), area = 0.3 in panel (b), and area = 0.09 in panel (c).]

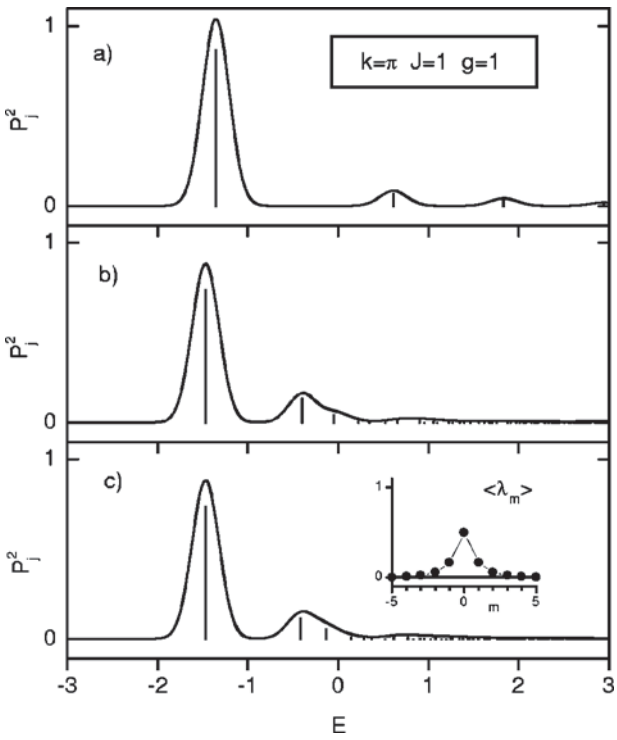

FIG. 6. Convergence of absorption spectra at the bottom of the band for $J=1$ and $g=1$. Panels (a), (b), and (c) show the results for the same basis sets as in Fig. 3. The area of the broadened spectra is normalized to 0.45.

Fig. 6(c). The energy of the lowest state changes from -1.46955 to -1.46961 and then agrees up to five significant figures with the results from Ref. 53.

For values of J much above 1, the Lang-Firsov basis becomes increasingly inefficient. While approaching the strong electronic coupling regime $J \gg g$, the lattice displacement is not localized around the exciton anymore in very contrast to the premises of our truncation scheme. In the strong coupling limit, the exciton hopping is ''fast'' compared to the exciton phonon coupling and the Born-Oppenheimer approximation should be applied to the whole crystal as one object (see Ref. 33). The total lattice displacement $\Sigma\langle\hat{\lambda}_m\rangle = g$ is now equally distributed over the $N\rightarrow\infty$ molecules. Therefore, the total relaxation energy $E_{\mathrm{FC}} = g^2\Sigma\langle\hat{\lambda}_m\rangle^2$ tends to zero. Figuratively speaking, the very fast exciton looses its phonon cloud. Compared to the molecular limit (lowest state at $E=0$), the lowest state will now be given by the purely electronic band at $E = 2J\cos k + g^2$. Because of the vanishing relaxation energy, higher vibronic states have no spectral weight and the absorption spectrum consists of a narrow line at the electronic energy.

IV. INCLUSION OF CT STATES

The Holstein Hamiltonian for Frenkel excitons (1) can be very naturally extended to include charge-transfer (CT) states. The relevance of CT states is a major point in the discussion of PTCDA and other quasi-one-dimensional crystals (see Sec. I). Let $c^{\dagger}_{n,f}$ be the creation operator for a nearest neighbor CT state in which an electron is transferred from lattice site n to site $n+f$ ($f=\pm 1$). The molecular limit is again defined as the case where no transfer interactions (neither Frenkel exciton transfer nor charge transfer nor Frenkel-CT interactions) are considered. Then, the electronic CT Hamiltonian is

$$H^{\mathrm{CT}} = D\sum_{n,f} c^{\dagger}_{n,f}c_{n,f}, \tag{44}$$

with D being the on-site energy of a CT state in the molecular limit (relative to the Frenkel exciton on-site energy at zero in our energy units).

The electron or hole excitation of the CT state are assumed to couple to the same effective vibrational coordinate λ as the Frenkel exciton. With the electron-phonon coupling constant g_e and the hole-phonon coupling constant g_h, the linear coupling between CT states and phonons is described by the Hamiltonian

$$H^{\text{CT-ph}} = \sum_{n,f} c^{\dagger}_{n,f}c_{n,f}[-g_h(b^{\dagger}_n + b_n) - g_e(b^{\dagger}_{n+f} + b_{n+f}) + g_h^2 + g_e^2]. \tag{45}$$

These expressions are analogous to the Frenkel-exciton-phonon coupling in Eq. (4). The term $g_h^2 + g_e^2$ is the vibrational relaxation energy of a CT state in the molecular limit.

As in Eq. (4), this term is added to align the on-site energy D of the CT states to its value in the molecular limit.

The mixing between Frenkel and CT excitons can be described by the Hamiltonian

$$H^{\text{FE-CT}}=\sum_n\ [t_e(a_n^\dagger c_{n,+1}+a_n^\dagger c_{n,-1}) + t_h(a_n^\dagger c_{n+1,-1}+a_n^\dagger c_{n-1,+1})+\text{H.c.}]. \quad (46)$$

The charge-transfer integrals t_e (t_h) describe the transfer of an individual electron (hole) between the site of a Frenkel exciton and its nearest neighbor (see Refs. 24, 25). We neglect the dispersion (hopping) of CT states since this would involve a simultaneous hop of two particles and is expected to be on a much smaller energy scale. Thus, the extended Holstein-Hamiltonian for Frenkel and CT excitons becomes

$$H_{\text{Hol}}^{\text{FCT}}=H_{\text{Hol}}^{\text{FE}}+H^{\text{CT}}+H^{\text{CT-ph}}+H^{\text{FE-CT}}. \quad (47)$$

This Hamiltonian corresponds to the dimer Hamiltonian used in Ref. 24.

A natural extension of the basis states $|n\underline{\nu}\rangle$ from Eq. (5) is obtained by including the new electronic degree of freedom f. The value $f=0$ shall denote the former Frenkel exciton basis states

$$[|nf\underline{\nu}\rangle]_{f=0}\equiv|n\underline{\nu}\rangle. \quad (48)$$

A Lang-Firsov-type basis for CT states ($f=\pm1$) is defined by

$$|nf\underline{\nu}\rangle\equiv\underbrace{c_{n,f}^\dagger|0^{\text{el}}\rangle}_{\text{elec}}\times\underbrace{\frac{1}{\sqrt{\nu_0!}}(b_n^\dagger-g_h)^{\nu_0}|\tilde{0}_n^h\rangle}_{g_h\text{ displaced on }n} \times\underbrace{\frac{1}{\sqrt{\nu_f!}}(b_{n+f}^\dagger-g_e)^{\nu_f}|\tilde{0}_n^e\rangle}_{g_e\text{ displaced on }n+f} \times\underbrace{\prod_{m\neq0,f}\frac{1}{\sqrt{\nu_m!}}(b_{n+m}^\dagger)^{\nu_m}|0_{n+m}\rangle}_{\text{undisplaced otherwise}}. \quad (49)$$

Here, $|\tilde{0}_n^h\rangle$ is a ground state oscillator function displaced by the hole-phonon coupling constant g_h and $|\tilde{0}_n^e\rangle$ is an oscillator function correspondingly displaced by g_e. $b_n^\dagger-g_h$ and $b_n^\dagger-g_e$ create phonon excitations in these displaced oscillators.

The real-space basis states from Eq. (49) can again be Fourier transformed to momentum-space basis states with total momentum k:

$$|kf\underline{\nu}\rangle\equiv\frac{1}{\sqrt{N}}\sum_n\ e^{ikn}|nf\underline{\nu}\rangle. \quad (50)$$

As for the Frenkel problem, the matrix elements of the Frenkel-CT Holstein Hamiltonian (47) can be derived in a straightforward way. The final expressions become lengthy due to various overlap factors and we omit them here. The basis can be reduced to a manageable size by a truncation scheme as for the Frenkel problem. Then, the eigenstates $|\Psi_j(k)\rangle$ at $k=0$ or $k=\pi$ can again be obtained by standard diagonalization methods for real matrices.

From the eigenstates, the transition dipole moments can be reduced to the transition moments of the basis states. The Frenkel excitons $a^\dagger|0\rangle$ give rise to a Frenkel transition dipole operator as in Sec. II C:

$$\hat{P}_{\text{FE}}(q)=\frac{1}{\sqrt{N}}\sum_n\ e^{-iqn}(a_n^\dagger+a_n). \quad (51)$$

An equivalent operator can be introduced for CT states. In this case, the most elementary excitation always involves a unit of two molecules at n and $n\pm1$. As argued in Ref. 25, the symmetric CT excitation

$$\frac{1}{\sqrt{2}}(c_{n,+1}^\dagger+c_{n+1,-1}^\dagger)|0\rangle$$

can have a significant transition dipole moment $\vec{p}_{\text{CT}}$. On the other hand, the transition dipole of the antisymmetric CT excitation

$$\frac{1}{\sqrt{2}}(c_{n,+1}^\dagger-c_{n+1,-1}^\dagger)|0\rangle$$

is strictly zero for symmetry reasons. Therefore, we analyze only the q-dependent symmetric CT transition operator

$$\hat{P}_{\text{CT}}(q)=\frac{1}{\sqrt{N}}\sum_n\ e^{-iqn}\left(\frac{c_{n,+1}^\dagger+c_{n+1,-1}^\dagger}{\sqrt{2}}+\text{H.c.}\right). \quad (52)$$

Then,

$$P_{\text{FE}j}(k)\equiv\langle\Psi_j(k)|\hat{P}_{\text{FE}}(k)|0^{\text{tot}}\rangle \quad (53)$$

gives the Frenkel part of the transition dipole along $\vec{p}_M$ and

$$P_{\text{CT}j}(k)\equiv\langle\Psi_j(k)|\hat{P}_{\text{CT}}(k)|0^{\text{tot}}\rangle \quad (54)$$

gives the CT part of the transition dipole along $\vec{p}_{\text{CT}}$. At $k=0$, the absolute transition dipole for absorption of visible light is obtained as

$$\vec{P}_j=P_{\text{FE}j}(0)\vec{p}_M+P_{\text{CT}j}(0)\vec{p}_{\text{CT}}. \quad (55)$$

These transition dipoles are now determined by two independent contributions. However, in a first approximation the CT transition dipole will be small and $\vec{P}_j$ will mainly be given by its Frenkel component. As for the Frenkel problem [see Eq. (19)], the k-dependent spectral weights $P_{\text{FE}j}^2(k)$ and $P_{\text{CT}j}^2(k)$ represent the electronic character (Frenkel or symmetric CT) of state j.

A representative calculation is shown in Figs. 7 and 8 for the parameters $J=0.5$, $g=1$, $D=0$, $t_e=t_h=0.5$. The Frenkel part of this parameter set corresponds to the calculation

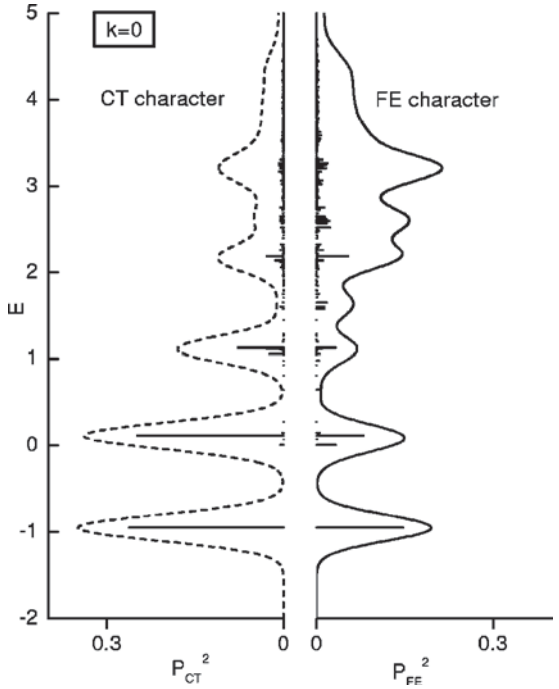

FIG. 7. Eigenstates of the extended Holstein model for Frenkel-CT mixing (47) at total momentum $k=0$. Parameters $J=0.5$, $g=1$, $D=0$, $t_e=t_h=0.5$, $g_e=g_h=1/\sqrt{2}$. The Frenkel parameters and the illustration correspond to Fig. 1. P^2_{FE} shows the spectral weights (Frenkel character) of the Frenkel-part, P^2_{CT} shows the spectral weights of the symmetric CT part. The broadened spectra are both normalized to an area of 0.5.

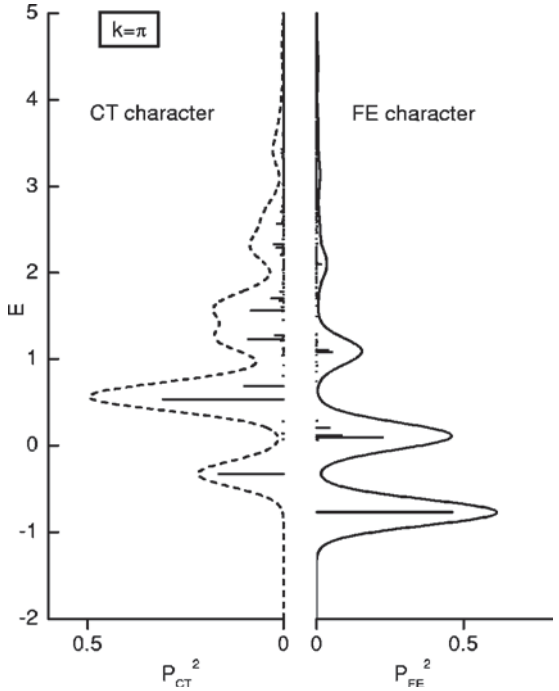

FIG. 8. Eigenstates of the extended Holstein model for Frenkel-CT mixing (47) at total momentum $k=\pi$. Parameters as in Fig. 7. Because of $t_e=t_h$, the electronic FE and CT states do not mix and all eigenstates have either pure FE or pure CT character.

in Fig. 1. The basis cut-off vector for the phonon-space was $|\underline{\nu}\rangle^{\max}=|1234\tilde{5}4321\rangle$ with $\nu^{\max}_{\mathrm{tot}}=5$, resulting in 4332 basis states. An additional CT state is assumed at resonance with the Frenkel state ($D=0$). The charge-transfer integrals t_e and t_h are chosen equal to the Frenkel hopping integral to give an illustration for strong Frenkel-CT mixing.

For the electron and hole coupling parameters, we used $g_e=g_h=g/\sqrt{2}$, which gives equal relaxation energy for the CT state and the Frenkel exciton. Perylene's π system is alternant. Simple Hückel theory then gives equal and opposite charges in the cation and anion, with half-filled HOMO and LUMO, respectively, while both are half-filled in the excited state. We have $g_e=g_h=g/2$ for noninteracting electrons. The Pariser-Parr-Pople model of interacting π electrons yields $g_e=g_h$ for systems with electron-hole symmetry. The bond order changes and relaxation energy of the singlet excitation in anthracene or trans-stilbene are now approximately half that of the triplet, which in turn is comparable to the relaxation energy of dication or dianion.[68,69] Our initial choice of equal relaxation energy for the Frenkel and CT excitation follows the correlated case, although this is a guess and PTCDA does not have e-h symmetry.

At the top of the band ($k=0$), the energetic degeneracy and the large charge-transfer integrals lead to a strong mixing of Frenkel and CT states throughout the whole spectrum. The overall distribution of the spectral weights gives more Frenkel character to the higher states as a result of the positive J. The FE character in Fig. 7 should be compared to the Frenkel-only problem from Fig. 1. In the Frenkel-only problem, the lowest state gave rise to a single peak in the broadened spectrum at $E\approx 0$. This peak is now split into two well separated peaks at $E\approx -1$ and $E\approx 0$. In such a way, strong mixing with CT states can add new features to the absorption spectrum even if their intrinsic transition dipoles are zero ($\vec{p}_{\mathrm{CT}}=0$). This phenomenon is commonly described by the figurative phrase that the CT states "borrow" oscillator strength from the Frenkel states.

At the bottom of the band ($k=\pi$, Fig. 8), the symmetry of the CT integrals ($t_e=t_h$) in this special case decouples the electronic Frenkel and CT states (see Ref. 24). Therefore, the spectral weight of all states has either pure Frenkel or pure CT character. Only some indirect mixing is introduced by the phonon part of the Hamiltonian, which mainly affects the vibronic structure of the CT-character states.

V. DESCRIPTION OF EXPERIMENTAL ABSORPTION SPECTRA

In Sec. IV, the energies E_j and transition dipoles P_j (55) of the eigenstates of the one-dimensional Holstein problem were obtained. These quantities are essential but not yet sufficient for the description of a real absorption spectrum of a quasi-one-dimensional molecular crystal. Let us first return from the dimensionless quantities E, J, D, t, and P to absolute values, which are denoted by a tilde to prevent confusion. The absolute excitation energy of state $|\Psi_j\rangle$ is then given by

$$\tilde{E}_j=\tilde{E}_{00}+E_j\cdot\hbar\omega, \tag{56}$$

where $\tilde{E}_{00}$ is the absolute energy of the lowest eigenstate with respect to the electronic and vibrational ground state of the crystal. Furthermore, we will only consider the Frenkel contribution to the transition dipoles in Eq. (55):

$$\tilde{\vec{P}}_j = \vec{p}_M \cdot P_{\mathrm{FE}j}. \tag{57}$$

In PTCDA and MePTCDI and many other organic crystals, the unit cell contains two nonequivalent molecules. We now assume that *all* interstack interactions are on a much smaller energy scale than the in-stack interaction J. That means, the energy spectrum of the one-dimensional model is in first approximation not affected. Only the transition dipoles of the two molecules A and B couple and form two Davydov components ($\beta = p,s$) with two orthogonal transition dipoles

$$\tilde{\vec{P}}_{j\beta} = \frac{\vec{p}_M(\mathrm{A}) \pm \vec{p}_M(\mathrm{B})}{\sqrt{2}} \cdot P_{\mathrm{FE}j}. \tag{58}$$

If φ is the angle between the two nonequivalent molecular transition dipoles, the absolute value of the Davydov components can be written as

$$\tilde{P}_{j\beta} = p_\beta \cdot P_{\mathrm{FE}j}, \tag{59}$$

with the transition dipoles per unit cell p_β:

$$p_p = p_M \cos\frac{\varphi}{2}, \tag{60}$$

$$p_s = p_M \sin\frac{\varphi}{2}. \tag{61}$$

For the crystal structure of PTCDA and MePTCDI, the p direction is given as the crystallographic b axis. The s direction lies approximately in the (102) plane because the molecular planes of both inequivalent molecules are roughly parallel to the (102) plane [within 5° (Ref. 70) for PTCDA and within 10° for MePTCDI, derived from Ref. 71].

Knowing the transition dipoles per unit cell, the transverse dielectric constant for perturbation by an external light wave polarized along the $\beta = p,s$ directions can be expressed as a sum over the excited states (see, e.g., Refs. 72, 73):

$$\epsilon_\beta^0(\tilde{E}) = 1 + \frac{8\pi}{v} p_\beta^2 \sum_j \frac{P_{\mathrm{FE}j}^2 \tilde{E}_j}{\tilde{E}_j^2 - \tilde{E}^2 - i\hbar\Gamma\tilde{E}}. \tag{62}$$

Here, v is the volume of the unit cell and Γ^{-1} the life time of the excited states.

Equation (62) is rigorous for any quantum system if *all* excited states are included. However, we are considering only the lowest electronic excitation. Therefore, we include the contribution of the higher states (mixing of molecular configurations) by using a phenomenologically modified formula for the dielectric function

$$\epsilon_\beta(\tilde{E}) = \epsilon_\beta^{\mathrm{bg}} + \frac{8\pi}{v} (f_\beta^{\mathrm{bg}} p_\beta)^2 \sum_j \frac{P_{\mathrm{FE}j}^2 \tilde{E}_j}{\tilde{E}_j^2 - \tilde{E}^2 - i\hbar\Gamma\tilde{E}}. \tag{63}$$

Here, $\epsilon_\beta^{\mathrm{bg}}$ is a background dielectric constant that represents the value of $\epsilon_\beta(0)$ corresponding to a crystal in which the considered lowest electronic excitation would not exist. f_β^{bg} is a screening factor describing the modification of the acting field by the higher transitions. Furthermore, the higher transitions will modify the Frenkel exciton hopping integral J and thereby all the eigenstates of the system. Since we treat J as an effective fitting parameter anyway, the effect of the higher transitions onto J is not important here but should be remembered in any microscopic interpretation of J. Such a background modification of the dielectric function was discussed for a simple model system of one purely electronic Frenkel exciton in a cubic crystal in Ref. 39. In our general case, the effect of the higher transitions represented in the background parameters is also anisotropic in nature.

The dielectric function (63) includes a Lorentzian broadening of the individual eigenstates due to a finite lifetime Γ^{-1}. In a typical situation, however, there are several other sources of a much larger broadening: (i) coupling to further low-energy vibrations, (ii) splitting of the main vibrational mode, which consists actually of several nearly degenerate modes, and (iii) inhomogeneous broadening. To account for all these effects empirically, we replace each eigenstate of the Holstein model $|\Psi_j\rangle$ by a Gaussian distribution of states with standard deviation σ_j as, e.g., done in Ref. 74. The individual broadenings σ_j have no microscopic meaning and should be seen as no more than a convenient tool to compare the spectrum from the eigenstates of the Holstein model to an experimental spectrum. Practically, we assigned constant values of σ_j for 4 separate regions of the spectrum in order to have only four different broadening parameters. The individual Lorentzian linewidth is assumed to be much smaller than the σ_j and does not contribute anymore.

From the complex dielectric function (63), the complex refractive index $(n + i\kappa)^2 = \epsilon$ and the absorption coefficient $\alpha = 2\tilde{E}/(\hbar c) \cdot \kappa$ can be calculated for the special light waves that propagate perpendicular to the p-s plane and are polarized along the p or s direction. For general directions, the complex rules of crystal optics would have to be considered.

For PTCDA, it is possible to create vapor-deposited polycrystalline films with a high preferential orientation such that the (102) crystal planes always lie parallel to the substrate. Furthermore, the anisotropy between the p and s direction is expected to be very small due to the almost right angle between the molecules ($\varphi = 82°$). Thus, $\epsilon_p \approx \epsilon_s$ can be directly probed by a vertical incidence absorption measurement on such films. For thicknesses above ≈ 30 nm, the influence of interface reflections and interference effects is small and the absorption coefficient follows directly from the optical density and the layer thickness. The layer thickness, however, is difficult to determine accurately. Haskal *et al.*[22] report absolute absorption coefficients for PTCDA on glass, deposited at low substrate temperature. We determined absolute absorption coefficients for PTCDA on mica at room temperature. The orientation of the (102) planes parallel to the substrate was verified by x-ray diffraction and the layer thicknesses (e.g., 30 nm) were determined by atomic force microscopic investigation of step profiles. Our results for the integral ab-

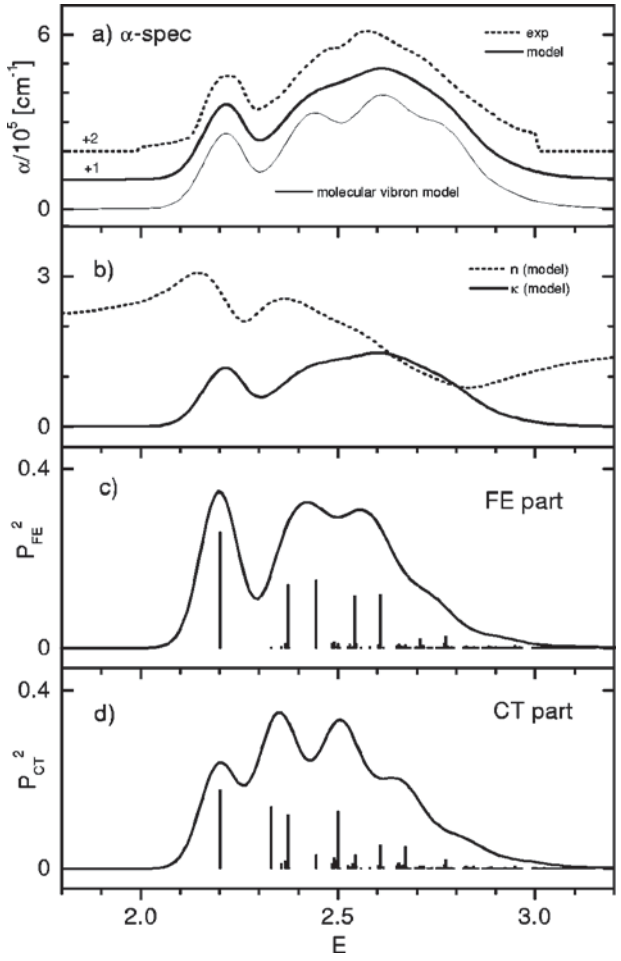

FIG. 9. Experimental low temperature absorption spectra of PTCDA and model fit. Panel (a) shows the comparison for the absorption coefficient α. The model fit (parameters see text) is done with a large phonon basis (as in Fig. 7) but a comparison with the molecular vibron model for the same parameters is also given. Panel (b) shows the optical constants n, κ corresponding to the model fit. Panel (c) shows the actual eigenstates and the Frenkel part of their spectral weight. In panel (d), the CT part of the spectral weight is given. The stick spectra are broadened by Gaussians with a constant width $\sigma=48$ meV corresponding to the width of the lowest state in the fit.

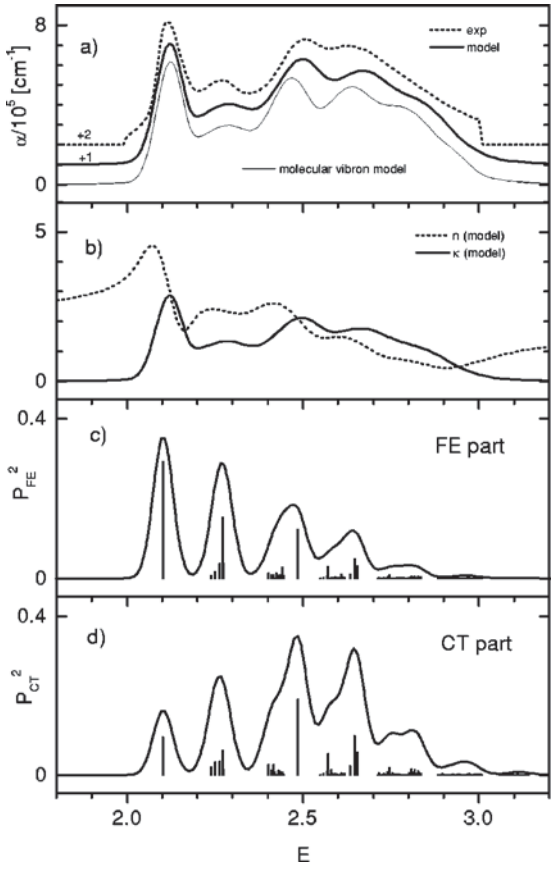

FIG. 10. Experimental absorption spectra of MePTCDI and model fit. Panel (a) shows the comparison for the p-polarized α spectra, the parameters are given in the text. The model spectrum is shown for a large phonon cloud basis (as in Fig. 7) and the molecular vibron model. Panel (b) gives the optical constants from the model. Panels (c) and (d) show the actual eigenstates and their composition as explained in Fig. 9. The broadening in (c) and (d) is constant $\sigma=28$ meV as for the lowest peak in the experimental spectrum. Due to the variable broadening in the fit, the second large peak at ≈ 2.3 eV from panel (c) appears in the α and κ spectra of panels (a) and (b) only as a broad feature with lower peak value.

sorption coefficient agree within 7% with the ones from Ref. 22. Using our value of $\int \alpha d\tilde{E}=2.2\times 10^{-5}$ cm^{-1} eV (in the range 2–3 eV), we calibrate the low-temperature absorption spectrum of PTCDA reported in Ref. 25 to absolute values. This spectrum is shown in Fig. 9(a).

For MePTCDI, the angle between the two nonequivalent molecules is $\varphi=37°$ (derived from Ref. 71) and thus the anisotropy between the p and s direction is expected to be strong ($p_p^2/p_s^2=9.0$). Polarized low-temperature absorption spectra of MePTCDI were reported in Ref. 25, but there the absolute scaling was not known. To provide an approximate scaling, we assume that the isotropic average of the integral absorption coefficient should equal that of PTCDA [$\int(\alpha_p+\alpha_s)d\tilde{E}=\int\alpha(\mathrm{PTCDA})d\tilde{E}$] since the molecular transition dipoles of the two materials are very similar[25] and only their crystal structure differs. The resultant p-polarized spectrum is shown in Fig. 10(a). At this stage, we do not intend to explain the dependence of the spectral shape on polarization. Such a dependence might be affected by contributions of a nonzero intrinsic CT transition dipole,[25] by nonzero interstack coupling,[27] and by the anisotropy of the dielectric background contribution. By concentrating on the p-polarized spectrum, at least the CT contribution would be minimized.

We note that the consideration of the *absolute* absorption coefficient is essential for describing the shape of solid state spectra. The microscopic models provide predictions only about the *relative* spectral distribution of the transition dipoles, which determines the shape of the imaginary part $\epsilon_2(\tilde{E})$ of the dielectric function. The shape of the absorption spectrum $\alpha(\tilde{E})$, however, is strongly influenced by the variation of the refractive index in the absorption region [$\alpha=\tilde{E}/(\hbar c)\cdot\epsilon_2/n$] and the variation of n is again determined

by the absolute absorption coefficient. Only if α is very small, as typically for spectroscopy of solutions, n does not vary and the shape of the absorption spectrum is directly given by the shape of the transition dipole distribution (''dilute limit''). The best approach would be, of course, to obtain the complex dielectric function from experiment. Such data is presently available only for films of unknown degree of orientational order.[75]

The dielectric function (63) allows a direct fit of the absorption spectra in which ϵ^{bg} and f^{bg} have to be considered as fitting parameters. ϵ^{bg} can be chosen from the independend criterion that the refractive index n below the absorption region is matched. For PTCDA, we used the value of $\epsilon(\tilde{E}=0.962\ \mathrm{eV})=4.07$.[76] For MePTCDI, the anisotropy in the (102) plane is not known. We use an estimate of $\epsilon(\tilde{E}=0.962\ \mathrm{eV})=4.66$ based on long and medium axis molecular polarizabilities of the PTCDA molecule[77,78] and the different relative orientations of MePTCDI. For such relatively large values of the low energy dielectric constant, the precise number does not affect the results.

The eigenstates of the Holstein model are determined by the parameters $\hbar\omega$, $\tilde{J}=J\cdot\hbar\omega$, g, $\tilde{E}_{00}$ for the Frenkel part and g_e, g_h, $\tilde{D}=D\cdot\hbar\omega$, $\tilde{t}_e=t_e\cdot\hbar\omega$, $\tilde{t}_h=t_h\cdot\hbar\omega$ for the Frenkel-CT mixing. We assume that the intramolecular vibrational quantum $\hbar\omega$ and its coupling g to the intramolecular excitation are not affected by the surrounding crystal and can be derived from the absorption spectrum of isolated molecules in solution. A fit of the solution spectrum of MePTCDI in $CHCl_3$ (Ref. 25) to a simple vibronic progression (with freely adjustable Gaussian broadenings) gives $\hbar\omega=0.17$ eV and $g=0.88$. We use the same values for PTCDA, since the absorption spectrum of PTCDA in CH_2Cl_2 from Ref. 79 is identical within graphical accuracy apart from an absolute energy shift of 23 meV. For the electron and hole coupling parameters we used $g_e=g_h=g/\sqrt{2}$ as in Sec. IV. Furthermore, we use only one charge-transfer integral $t=t_e=t_h$, since the electronic problem at $k=0$ is only determined by the sum t_e+t_h.[24,25] With these assumptions, four unknown empirical parameters remain in the Holstein model at $k=0$: $\tilde{J}$, $\tilde{E}_{00}$, $\tilde{D}$, and $\tilde{t}$. This freedom in the parameter space is still too large to obtain definite values from the absorption spectra alone. We determined parameter sets by global fitting procedures in order to find some relevant values that are useful to discuss the absorption spectra.

For PTCDA, a representative fitting result is shown as the model spectrum in Fig. 9(a) in comparison with the experimental spectrum. The parameters are $\tilde{J}=42$ meV, $\tilde{D}=97$ meV, $\tilde{t}=85$ meV, and $\tilde{E}_{00}=2.23$ eV. This parameter set corresponds to a strong mixing of Frenkel and CT excitons as can be seen from the FE and CT contributions shown in panels (c) and (d). The α spectrum follows roughly the absorption index κ in panel (b). The characteristic difference between the absorption (α) spectrum in 1(a) and the distribution of the spectral weight in 1(c) is entirely caused by the spectral shape of the refractive index n, which becomes small at energies above the major absorption region. The phonon basis for the model spectrum was chosen as in the calculations for Figs. 7 and 8. Additionally, we show a model spectrum for the same parameters (including the broadenings) but using the molecular vibron model. Molecular vibrons for the CT states are naturally defined by all configurations that allow phonons only at the site of the electron or the hole. The comparison with the large phonon basis shows almost no differences apart from the larger broadening in the large basis. This close resemblance is mainly caused by the relatively small values of the transfer integrals and a coupling constant $g\approx 1$. Thus, at least for the Frenkel part of the problem, the parameters are close to the scenario of Fig. 2(b), where the molecular vibron model becomes exact.

We emphasize that similarly good fits of the experimental spectra can be obtained for different parameter sets with varying degree of CT mixing. Even total neglect of CT states would give a satisfactory fit with a Frenkel transfer integral of 70 meV. Such a value corresponds to the three-dimensional Frenkel exciton model for PTCDA in Ref. 27 with a nearest-neighbor hopping of 82 meV.

For MePTCDI, a fitting result is shown in Fig. 10(a). The parameters are $\tilde{J}=46$ meV, $\tilde{D}=240$ meV, $\tilde{t}=115$ meV, and $\tilde{E}_{00}=2.13$ eV. As for PTCDA, the obtained parameter set represents a strong mixing of Frenkel and CT excitons. Since the spectrum of MePTCDI shows a more pronounced peak structure, there is not as much freedom in choosing the parameters. In particular, only the inclusion of the CT states can reproduce the typical shape with four pronounced peaks. In contrast to the fit for PTCDA, in MePTCDI the molecular vibron model shows visible differences compared the large phonon basis. Nevertheless, it captures the situation accurately enough regarding the overall uncertainty of the interpretation.

VI. DISCUSSION

In this article, we modeled absorption spectra and dielectric responses of molecular crystals in the simplest context of a one-dimensional Holstein model. Our procedure for constructing $k=0$ or $k=\pi$ states with a tailored basis is general and also appropriate for models with more coupled modes or more electronic states. However, the computational effort increases dramatically in particular with the number of modes. Practically, only the regime of weak up to intermediate electronic coupling can be calculated at sufficient accuracy. For strong electronic coupling, the underlying concept of a localized phonon cloud becomes inappropriate.

We used this approach to model absorption spectra of two closely related molecular crystals (MePTCDI and PTCDA). At the present stage, the comparison between models and experimental data still involves serious compromises. The model neglects or approximates several effects whose influence is not accurately known: (i) three-dimensional Frenkel exciton hopping, (ii) coupling to several vibrational modes, and (iii) mixing of higher electronic states. In spite of these simplifications, the model still contains too many parameters to derive unique values alone from the optical absorption spectra. Our present parameters are meant to illustrate spectroscopic applications of Holstein models to actual materials, but their precise magnitudes remain to be found.

We used microscopic arguments to derive the exciton-phonon coupling constants g, g_e, g_h from solution spectra of isolated molecules. The inclusion of charge-transfer states is motivated (i) by the strong and nearly isotropic electroabsorption response of PTCDA (as in the interpretation of Ref. 24), (ii) by the polarization dependence of MePTCDI spectra,[25] and (iii) by the detailed structure of the MePTCDI spectrum, which demands extensions of the pure Frenkel exciton Hamiltonian from Eq. (1). As a guiding principle, we tried to explain two related compounds within the same scheme. This favors our present choice with similar exciton hopping integrals for PTCDA and MePTCDI. In addition, we concentrated on low-temperature absorption spectra. These show some structure even for the broad high-energy absorption band of PTCDA (2.3−2.9 eV).

The differences between the scenario presented here and other recent interpretations results from the inclusion of different aspects. In Ref. 24, a comprehensive picture was given for absorption, emission, and electroabsorption of PTCDA. The underlying model Hamiltonian was identical with our present one [Eq. (46)] but the $k=0$ states were calculated within a dimer approximation. Furthermore, the absorption spectrum was approximated in the dilute limit without using a dielectric function. The obtained key parameters in Ref. 24 are $\tilde{J}=180$ meV, $\tilde{D}=22$ meV, and $(\tilde{t}_e+\tilde{t}_h)/2=89$ meV. The larger value of $\tilde{J}$ mainly results from the assignment of the strongly redshifted emission spectrum. Furthermore, the inclusion of the dielectric function would redistribute spectral weight in the absorption spectrum to higher energies. This solid state effect is not included in Ref. 24 and thus is compensated by a larger value of $\tilde{J}$. The general picture of strong Frenkel-CT mixing caused by a Frenkel-CT separation $\tilde{D}$ in the same order as the charge-transfer integrals $\tilde{t}$ corresponds to our present study.

In Ref. 25, a model was used that considered Frenkel-CT mixing as in our present study and some extensions for three-dimensional crystals. The effect of the dielectric function was approximately included by the way of extracting the transition dipoles from the spectra. However, the Hamiltonian was explicitly constructed within the molecular vibron model and the vibronic replicas of the CT states were neglected. The obtained key parameters for MePTCDI are $\tilde{J}=110$ meV, $\tilde{D}=-80$ meV, and $(\tilde{t}_e+\tilde{t}_h)/2=50$ meV. Because of the severe simplifications, the overall shape of the spectra and the CT position $\tilde{D}$ were only very roughly described. The emphasis in Ref. 25 lay on the observed polarization ratios and Davydov splittings. Both effects are still beyond the presently studied Hamiltonian. The mixing of Frenkel and CT states, which was supported by the polarization ratios, agrees qualitatively with the present study.

In Ref. 26, a three-dimensional crystal model with Frenkel and several CT excitons is used for absorption and electroabsorption spectra of PTCDA and MePTCDI. The molecular vibron model was used as in Ref. 25 and the absorption spectrum was calculated for the dilute limit as in Ref. 24. The overall outcome is a significant Frenkel-CT mixing with, e.g., $\tilde{J}=200$ meV, $\tilde{D}=120$ meV, and $(\tilde{t}_e+\tilde{t}_h)/2=90$ meV for MePTCDI.

In Ref. 27, a three-dimensional Frenkel-exciton Hamiltonian within the molecular vibron approximation and a dielectric function model were used for modeling optical constants of PTCDA. The resulting nearest-neighbor Frenkel exciton transfer integral is $\tilde{J}=82$ meV. Polarization ratios and Davydov splittings of PTCDA were explained by the three-dimensional Frenkel interactions, which are beyond our present study. The proposed value of $\tilde{J}$ agrees with our model for PTCDA if we would neglect CT states (see Sec. V).

In our present study, the changes of the absorption spectra in the solid state compared to the much narrower solution spectra are mainly caused by the dielectric function model, by the mixing with CT states and—to a smaller degree—by the positive Frenkel hopping integral. All three effects distribute spectral weight in the absorption spectrum to a higher energy region. The Frenkel-CT mixing and the inclusion of separated exciton-phonon configurations explain the tendency towards spectra with more features spread over a wide energy range. The scenario of Frenkel-CT mixing corresponds roughly to Refs. 24, 25, or 26. We emphasize that the Frenkel-CT mixing in our study is only manifested in the detailed structure of the MePTCDI spectrum.

Obviously, the exact situation and reliable parameter values can only be obtained if all relevant effects are included in one model: separated exciton-phonon configurations, three-dimensional interactions, the possibility of Frenkel-CT mixing, a dielectric model and mixing with higher states. In order to determine the multitude of arising parameters, a broad set of experimental information has to be obtained and critically used.

The major goal of this article was to investigate the structure of phonon clouds for molecular crystals of current interest, in which the exciton-phonon coupling constant typically is in the order of 1. We illustrated that the molecular vibron model [Eq. (26)] with joint exciton-phonon configurations is justified only for $g\approx 1$ and $J\ll 1$. This regime is approximately realized in our interpretation of PTCDA and MePTCDI spectra ($J\approx 0.27$). For larger values of J, the effects of delocalized phonon clouds become significant (see Figs. 3 and 4 for $J=0.5$). Such larger values are also used for PTCDA in the literature, and they are of interest for many other applications. In these cases, an extended phonon cloud basis should be used for the calculation of the vibronic states.

ACKNOWLEDGMENTS

We thank V. M. Agranovich and E. Tsiper for stimulating discussions on the local field method and dielectric properties. We are grateful to J. Bonča for providing data from Ref. 53 in electronic form. We gratefully acknowledge partial support from the National Science Foundation through the MRSEC program under Grant No. DME-9400362.

*Corresponding author. Present address: Institut für Angewandte Photophysik, TU Dresden, 01062 Dresden, Germany. Email address: mi-hoffm@iapp.de

[1] C. W. Tang and S. A. VanSlyke, Appl. Phys. Lett. **51**, 913 (1987).
[2] J. H. Burroughes, D. D. C. Bradley, A. R. Brown, R. N. Marks, K. Mackay, R. H. Friend, P. L. Burns, and A. B. Holmes, Nature (London) **347**, 539 (1990).
[3] M. A. Baldo, D. F. O'Brien, Y. You, A. Shoustikov, S. Sibley, M. E. Thompson, and S. R. Forrest, Nature (London) **395**, 151 (1998).
[4] R. H. Friend, R. W. Gymer, A. B. Holmes, J. H. Burroughes, R. N. Marks, C. Taliani, D. D. C. Bradley, D. A. Dos-Santos, J. L. Brédas, M. Loglund, and W. R. Salaneck, Nature (London) **397**, 121 (1999).
[5] J. Huang, M. Pfeiffer, A. Werner, J. Blochwitz, S. Liu, and K. Leo, Appl. Phys. Lett. **80**, 139 (2002).
[6] C. W. Tang, Appl. Phys. Lett. **48**, 183 (1986).
[7] P. Peumans, V. Bulovic, and S. R. Forrest, Appl. Phys. Lett. **76**, 2650 (2000).
[8] J. H. Schön, C. Kloc, E. Bucher, and B. Batlogg, Nature (London) **403**, 408 (2000).
[9] D. Meissner and J. Rostalski, Synth. Met. **121**, 1551 (2001).
[10] J. H. Schön, C. Kloc, and B. Batlogg, Synth. Met. **124**, 95 (2001).
[11] J. H. Schön, C. Kloc, and B. Batlogg, Phys. Rev. Lett. **86**, 3843 (2001).
[12] J. H. Schön, C. Kloc, and B. Batlogg, J. Appl. Phys. **90**, 3419 (2001).
[13] J. Schön, C. Kloc, and B. Batlogg, Science **288**, 2338 (2000).
[14] J. Schön, C. Kloc, A. Dodabalapur, and B. Batlogg, Science **289**, 599 (2000).
[15] J. H. Schön, C. Kloc, and B. Batlogg, Science **293**, 2432 (2001).
[16] J. H. Schön, C. Kloc, R. C. Haddon, and B. Batlogg, Science **288**, 656 (2000).
[17] T. Holstein, Ann. Phys. (N.Y.) **8**, 325 (1959).
[18] T. Holstein, Ann. Phys. (N.Y.) **8**, 343 (1959).
[19] S. R. Forrest, Chem. Rev. **97**, 1793 (1997).
[20] E. Umbach, K. Glöckler, and M. Sokolowski, Surf. Sci. **402-404**, 20 (1998).
[21] P. M. Kazmaier and R. Hoffmann, J. Am. Chem. Soc. **116**, 9684 (1994).
[22] E. I. Haskal, Z. Shen, P. E. Burrows, and S. R. Forrest, Phys. Rev. B **51**, 4449 (1995).
[23] V. Bulovic, P. E. Burrows, S. R. Forrest, J. A. Cronin, and M. E. Thompson, Chem. Phys. **210**, 1 (1996).
[24] M. H. Hennessy, Z. G. Soos, R. A. Pascal, Jr., and A. Girlando, Chem. Phys. **245**, 199 (1999).
[25] M. Hoffmann, K. Schmidt, T. Fritz, T. Hasche, V. M. Agranovich, and K. Leo, Chem. Phys. **258**, 73 (2000).
[26] G. Mazur, Ph.D. thesis, Jagiellonian University, Cracow, 2001.
[27] I. Vragovic, R. Scholz, and M. Schreiber, Europhys. Lett. **57**, 288 (2002).
[28] M. Sadrai, L. Hadel, R. R. Sauers, S. Husain, K. Krogh-Jespersen, J. D. Westbrook, and G. R. Bird, J. Phys. Chem. **96**, 7988 (1992).
[29] M. Adachi, Y. Murata, and S. Nakamura, J. Phys. Chem. **99**, 14 240 (1995).
[30] R. Scholz, A. Y. Kobitski, T. U. Kampen, M. Schreiber, D. R. T. Zahn, G. Jungnickel, M. Elstner, M. Sternberg, and T. Frauenheim, Phys. Rev. B **61**, 13659 (2000).
[31] M. H. Hennessy, Z. G. Soos, V. Bulovic, and S. R. Forrest, in *Electrical, Optical, and Magnetic Properties of Organic Solid-State Materials IV*, edited by J. R. Reynolds *et al.,* MRS Symposia Proceedings No. 488 (Materials Research Society, Pittsburgh, 1998), p. 171.
[32] G. Klebe, F. Graser, E. Hädicke, and J. Berndt, Acta Crystallogr., Sect. B: Struct. Sci. **45**, 69 (1989).
[33] W. T. Simpson and D. L. Peterson, J. Chem. Phys. **26**, 588 (1957).
[34] D. P. Craig and S. H. Walmsley, *Excitons in Molecular Crystals* (Benjamin, New York, 1968).
[35] I. G. Lang and Y. A. Firsov, Sov. Phys. JETP **43**, 1843 (1962).
[36] R. E. Merrifield, J. Chem. Phys. **40**, 445 (1964).
[37] J. Appel, in *Solid State Physics. Advances in Research and Applications*, Vol. 21, edited by F. Seitz, D. Turnbull, and H. Ehrenreich (Academic Press, New York, 1968), Chap. 3, pp. 193–391.
[38] M. I. Klinger, *Problems of Linear Electron (Polaron) Transport Theory in Semiconductors* (Pergamon Press, Oxford, 1979).
[39] V. M. Agranovich and M. D. Galanin, *Electronic Excitation Energy Transfer in Condensed Matter* (North-Holland Publishing Company, Amsterdam, 1982).
[40] H. Böttger and V. V. Bryskin, *Hopping Conduction in Solids* (VCH, Weinheim, 1985).
[41] E. A. Silinsh and V. Čápek, *Organic Molecular Crystals. Interaction, Localization, and Transport Phenomena* (AIP Press, New York, 1994).
[42] D. R. Yarkony and R. Silbey, J. Chem. Phys. **67**, 5818 (1977).
[43] P. O. J. Scherer, E. W. Knapp, and S. F. Fischer, Chem. Phys. Lett. **106**, 191 (1984).
[44] Y. Zhao, D. W. Brown, and K. Lindenberg, J. Chem. Phys. **106**, 5622 (1997).
[45] A. H. Romero, D. W. Brown, and K. Lindenberg, Phys. Rev. B **60**, 4618 (1999).
[46] A. H. Romero, D. W. Brown, and K. Lindenberg, Phys. Rev. B **60**, 14 080 (1999).
[47] A. H. Romero, D. W. Brown, and K. Lindenberg, Phys. Rev. B **59**, 13 728 (1999).
[48] A. H. Romero, D. W. Brown, and K. Lindenberg, J. Lumin. **83-84**, 147 (1999).
[49] A. S. Alexandrov, V. V. Kabanov, and D. K. Ray, Phys. Rev. B **49**, 9915 (1994).
[50] G. Wellein, H. Röder, and H. Fehske, Phys. Rev. B **53**, 9666 (1996).
[51] G. Wellein and H. Fehske, Phys. Rev. B **56**, 4513 (1997).
[52] G. Wellein and H. Fehske, Phys. Rev. B **58**, 6208 (1998).
[53] J. Bonča, S. A. Trugman, and I. Batistiá, Phys. Rev. B **60**, 1633 (1999).
[54] H. De Raedt and A. Lagendijk, Phys. Rev. Lett. **49**, 1522 (1982).
[55] H. De Raedt and A. Lagendijk, Phys. Rev. B **27**, 6097 (1983).
[56] H. De Raedt and A. Lagendijk, Phys. Rev. B **30**, 1671 (1984).
[57] P. E. Kornilovitch and E. R. Pike, Phys. Rev. B **55**, R8634 (1997).
[58] E. Jeckelmann and S. R. White, Phys. Rev. B **57**, 6376 (1998).
[59] M. R. Philpott, J. Phys. Chem. **55**, 2039 (1971).
[60] R. E. Merrifield, Radiat. Res. **20**, 154 (1963).
[61] P. O. J. Scherer and S. F. Fischer, Chem. Phys. **86**, 269 (1984).
[62] N. Lu and S. Mukamel, J. Chem. Phys. **95**, 1588 (1991).
[63] F. C. Spano and S. Siddiqui, Chem. Phys. Lett. **314**, 481 (1999).
[64] F. C. Spano, J. Chem. Phys. **116**, 5877 (2002).
[65] P. M. Morse and H. Feshbach, *Methods of Theoretical Physics* (McGraw-Hill, New York, 1953).

[66] V. L. Broude, E. I. Rashba, and E. F. Sheka, *Spectroscopy of Molecular Excitons* (Springer-Verlag, Berlin, 1985).
[67] D. P. Craig, J. Chem. Soc. **1955**, 2302.
[68] Z. G. Soos, S. Ramasesha, D. S. Galvão, and S. Etemad, Phys. Rev. B **47**, 1742 (1993).
[69] S. Ramasesha, D. S. Galvão, and Z. G. Soos, J. Phys. Chem. **97**, 2823 (1993).
[70] M. Möbus, N. Karl, and T. Kobayashi, J. Cryst. Growth **116**, 495 (1992).
[71] E. Hädicke and F. Graser, Acta Crystallogr., Sect. C: Cryst. Struct. Commun. **42**, 189 (1986).
[72] F. Wooten, *Optical Properties of Solids* (Academic Press, New York, 1972).
[73] A. S. Davydov, *Theory of Molecular Excitons* (Plenum Press, New York, 1971).
[74] R. Brendel, J. Appl. Phys. **71**, 1 (1992).
[75] A. B. Djurisic, T. Fritz, and K. Leo, Opt. Commun. **183**, 123 (2000).
[76] D. Y. Zang, F. F. So, and S. R. Forrest, Appl. Phys. Lett. **59**, 823 (1991).
[77] Z. G. Soos, E. V. Tsiper, and R. A. Pascal, Jr., Chem. Phys. Lett. **342**, 652 (2001).
[78] E. V. Tsiper and Z. G. Soos, Phys. Rev. B **64**, 195124 (2001).
[79] U. Gomez, M. Leonhardt, H. Port, and H. C. Wolf, Chem. Phys. Lett. **268**, 1 (1997).